BBA - Biomembranes 1862 (2020) 183314

Contents lists available at ScienceDirect

BBA - Biomembranes

journal homepage: www.elsevier.com/locate/bbamem

DIBMA nanodiscs keep α-synuclein folded

Regina Adão[a], Pedro F. Cruz[b], Daniela C. Vaz[b,c], Fátima Fonseca[d,e], Jannik Nedergaard Pedersen[f], Frederico Ferreira-da-Silva[d,e], Rui M.M. Brito[b], Carlos H.I. Ramos[g], Daniel Otzen[f], Sandro Keller[h], Margarida Bastos[a,*]

[a] CIQ-UP, Departamento de Química e Bioquímica, Faculdade de Ciências, Universidade do Porto, Portugal
[b] UC-NMR & Coimbra Chemistry Centre, Chemistry Department, University of Coimbra, Portugal
[c] Centre for Innovative Care and Health Technology, School of Health Sciences, Polytechnic Institute of Leiria, Portugal
[d] i3S – Instituto de Investigação e Inovação em Saúde, Portugal
[e] Instituto de Biologia Molecular e Celular, Universidade do Porto, Portugal
[f] iNANO, Interdisciplinary Nanoscience Center, Aarhus University, Denmark
[g] Institute of Chemistry, University of Campinas-UNICAMP, Brazil
[h] Molecular Biophysics, Technische Universität Kaiserslautern (TUK), Germany

ARTICLE INFO

Keywords:
α-Synuclein
Membrane lipids
DIBMA
Lipid nanodiscs
DIBMALPs
Secondary structure

ABSTRACT

α-Synuclein (αsyn) is a cytosolic intrinsically disordered protein (IDP) known to fold into an α-helical structure when binding to membrane lipids, decreasing protein aggregation. Model membrane enable elucidation of factors critically affecting protein folding/aggregation, mostly using either small unilamellar vesicles (SUVs) or nanodiscs surrounded by membrane scaffold proteins (MSPs). Yet SUVs are mechanically strained, while MSP nanodiscs are expensive. To test the impact of lipid particle size on α-syn structuring, while overcoming the limitations associated with the lipid particles used so far, we compared the effects of large unilamellar vesicles (LUVs) and lipid-bilayer nanodiscs encapsulated by diisobutylene/maleic acid copolymer (DIBMA) on αsyn secondary-structure formation, using human-, elephant- and whale -αsyn. Our results confirm that negatively charged lipids induce αsyn folding in h-αsyn and e-αsyn but not in w-αsyn. When a mixture of zwitterionic and negatively charged lipids was used, no increase in the secondary structure was detected at 45 °C. Further, our results show that DIBMA/lipid particles (DIBMALPs) are highly suitable nanoscale membrane mimics for studying αsyn secondary-structure formation and aggregation, as folding was essentially independent of the lipid/protein ratio, in contrast with what we observed for LUVs having the same lipid compositions. This study reveals a new and promising application of polymer-encapsulated lipid-bilayer nanodiscs, due to their excellent efficiency in structuring disordered proteins such as αsyn into nontoxic α-helical structures. This will contribute to the unravelling and modelling aspects concerning protein-lipid interactions and α-helix formation by αsyn, paramount to the proposal of new methods to avoid protein aggregation and disease.

1. Introduction

α-Synuclein (αsyn) is a protein involved in the coordination of synaptic events, acting as a molecular monitor of the physiological changes at nerve terminals [1–5]. Conformational changes and aggregation of αsyn are related to deleterious effects of Parkinson's disease (PD) [1–3,5]. αsyn was first isolated from electric *Torpedo* fish and is reversibly associated with presynaptic vesicles of nervous terminals [3,4]. In the N-terminus of the αsyn sequence of vertebrates, the first 60 amino acids comprise 7 imperfect 11-residue repeats, containing variants of the consensus 6-residue sequence KTKEGV. These repeats are predicted to fold into an amphipathic α-helical structure resembling apolipoprotein when bound to membrane lipids [6,7], suggesting a lipid-binding activity for the N-domain. αsyn is a cytosolic protein that is natively unfolded (intrinsically disordered), with the N-terminal lipid binding domain having a weak preference for helical structure [8] and its assembly and folding depending on the surroundings.

From numerous studies on the role of lipids in αsyn folding and induction/inhibition of its aggregation, the main conclusion is that αsyn folding and aggregation are complex and highly sensitive to external conditions [8–16]. Nonetheless, it is known that αsyn efficiently binds to anionic lipid particles, and this induces the formation of α-

* Corresponding author.
E-mail address: mbastos@fc.up.pt (M. Bastos).

https://doi.org/10.1016/j.bbamem.2020.183314
Received 23 October 2019; Received in revised form 10 April 2020; Accepted 13 April 2020
Available online 15 April 2020
0005-2736/

helical structure and affects protein aggregation [11,17]. Studies carried out both with biological and synthetic lipids have shown that αsyn preferably interacts with small diameter phospholipids vesicles in the fluid phase [9–11,17,18], data consistent with the role attributed to the protein at the presynaptic level. Thus, lipids are known to play a role in the formation and stabilization of the alpha-helical secondary structural elements of the protein, avoiding structural transition to β-rich structures, with high tendency to aggregate [12–14,19–22]. In turn, aggregation of αsyn leads to both cytotoxic prefibrillar oligomers and amyloid fibrils [23–25]. Therefore, suppressing αsyn aggregation is a promising therapeutic approach in PD and other synucleinopathies [26–28]. Hence, unravelling and modelling aspects concerning protein-lipid interactions and α-helix formation by αsyn is paramount to propose new methods to avoid protein aggregation and disease.

So far, model membrane studies have mainly used either small unilamellar vesicles (SUVs) or nanodiscs surrounded by membrane scaffold protein (MSPs) [11,17,29–34], while fewer studies have been performed using large unilamellar vesicles (LUVs) [35,36]. SUVs are metastable, rearranging within a few days to form larger liposomes, while MSP nanodiscs demand additional protein production, which makes them quite costly. LUVs are mechanically stable and cheap, but their relatively large size poses challenges to optical spectroscopy in the far-UV range. An additional potential complication arises from the fact that αsyn itself can form discoidal lipoprotein nanodiscs by reshaping membrane lipids [13,37–40].

To overcome the limitations associated with the lipid particles used so far, as well as to test the impact of different lipid particle sizes, we set out to investigate the effects on αsyn secondary structure of either LUVs or lipid-bilayer nanodiscs formed by diisobutylene/maleic acid copolymer (DIBMA). DIBMA copolymers are able to entrap lipids from liposomes, producing well-defined and stable lipid nanodiscs referred to as DIBMA/lipid particles (DIBMALPs) [41–47]. We used LUVs of DPPC:DMPS 8:2 to produce DIBMALPs as the melting temperature of this lipid mixture (which is arguably the most important physical parameter of a membrane lipid) is within a range that is experimentally accessible for DSC studies. Thus, the ability to switch from the gel to the liquid phase provides important information about the nature of the interactions between lipids and proteins and allows us to assess possible differences in phase behavior between liposomes and the lipid nanodiscs used.

In order to assess differences in behavior depending on sequence, we further studied in parallel αsyn folding of the human αsyn (h-αsyn) with those from two mammal species of long lifespan: African elephant (*Loxodonta africana*) with a lifespan of 65 years (e-αsyn) and bowhead whale (*Balaena mysticetus*), the mammal with the longest longevity of > 200 years (w-αsyn) [48–50]. αsyn variants of these three species show a well-conserved sequence (Fig. 1) suggesting that the synucleins are also required for synaptic transmission and membrane trafficking in these species [4,51,52]. However, the three different αsyn variants show very different propensities to bind to and fold on DMPG LUVs [53], making it of interest to study their differences in interaction with DIBMALPs. Our results confirm that negatively charged lipids induce αsyn folding, and more importantly, they show that DIBMA/lipid particles (DIBMALPs) are highly efficient in promoting α-helix formation in all αsyn variants.

2. Experimental section

2.1. Preparation of liposomes

1,2-Dipalmitoyl-*sn*-glycero-3-phosphocholine (DPPC) and 1,2-dimyristoyl-sn-glycero-3-[phospho-L-serine] (DMPS) (Avanti Polar Lipids, Alabama, USA) were mixed for the preparation of DMPS and DPPC:DMPS (8:2) liposomes. The lipids were solubilized in an azeotropic mixture of chloroform:methanol (87:13, *v*/v), and the solvent was removed in a rotary evaporator to form a film that was dried under vacuum overnight. The lipid films were then hydrated at 50 °C for 30 min and resuspended to a concentration of 5 mM in buffer (50 mM phosphate, 50 mM NaF buffer, pH 7.4) by 3 vortex/freeze–thaw cycles (using liquid nitrogen and a water bath at 50 °C) to form multilamellar vesicles (MLVs). NaF was used instead of NaCl to ensure a low absorbance in the far-UV range. LUVs were obtained from MLVs by extrusion in a 10-mL stainless steel extruder (Lipex Biomembranes Inc. Vancouver, Canada) thermostated at 50 °C. The samples were passed 20 times through two superimposed polycarbonate filters (Whatman, Nucleopore, NJ, USA) with a pore size of 100 nm under an inert (N_2) atmosphere.

2.2. Preparation of nanodiscs

Lipid nanodiscs were prepared using DPPC:DMPS (8:2) liposomes and DIBMA copolymer solution. The DIBMA solution was dialysed against 2 L of the same buffer using a 3.5-kDa MWCO dialysis membrane (Spectrum Laboratories, Rancho Dominguez, USA) for 24 h at 25 °C, with buffer exchange after 16 h. Dialysed copolymer was filtered through 0.2-μm PTFE filters (GE Healthcare), and the concentration was measured in a refractometer Abbemat 300 instrument (Anton Paar, Graz, Austria) using the previously reported value of dn/dc 1.346 M^{-1} [46]. Nanodiscs were prepared by adding the polymer solution to the liposomes that were prepared in the same buffer, using always a molar ratio of $C_{(DIBMA)}/C_{(DPPC:DMPS)}$ = 0.3 and lipid concentrations between 0.25 and 4.5 mM. These mixtures were incubated for 16 h at 40 °C. To check for possible effects of excess unbound polymer in the nanodiscs solution, some nanodiscs samples were centrifuged at 15,000*g*, using an Amicon Ultra-4 100k centrifugal filters of 0.5 mL, at 40 °C, as the free polymer passes the filter, whereas the nanodiscs are retained. CD

Fig. 1. Sequence alignment of human, elephant, and whale αsyn. (Obtained using Clustal Omega) [54].

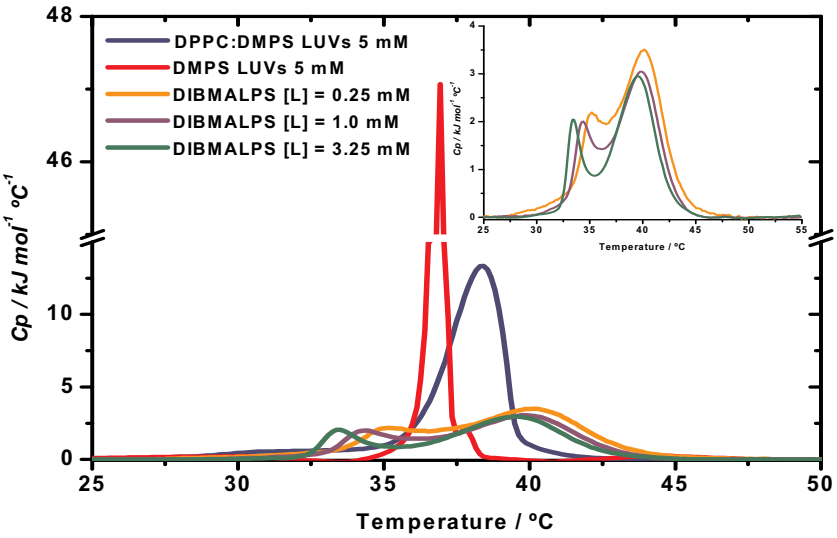

Fig. 2. Thermal profile of the various lipid systems LUVs of DMPS, DPPC:DMPS (8:2), and DIBMALPs prepared from DPPC:DMPS (8:2) LUVs. The DSC curves for DIBMALPs are also presented in the insert with an enlarged y-axis scale. DIBMALPs were prepared with 0.25, 1.0 and 3.25 mM lipid concentrations, but always at a constant polymer/lipid ratio, $C_{(DIBMA)}/C_{(DPPC:DMPS)} = 0.3$.

Table 1
Thermodynamic parameters measured by DSC for the gel-to-fluid phase transition of DMPS, DPPC:DMPS 8:2, and DIBMALPs in the absence of αsyn.

Parameters	T_{m1}[a] °C	T_{m2}[a] °C	ΔH_1 $kJ\,mol^{-1}$	ΔH_2 $kJ\,mol^{-1}$
DMPS	36.9		28.8	–
DPPC:DMPS 8:2	38.3		36.2	–
DIBMALPs[b]				
0.25 mM	35.4	40.0	6.3	16.2
1.0 mM	34.6	39.6	5.4	14.5
3.25 mM	33.6	39.3	3.8	13.9

[a] The uncertainty in T_m is estimated to be ± 0.3 °C and in ΔH ± 0.8 kJ mol^{-1}.
[b] For DIBMALPs, the ratio $C_{(DIBMA)}/C_{(DPPC:DMPS)} = 0.3$ was always used. The table shows the lipid concentrations in each case.

experiments were performed with both centrifuged and non-centrifuged samples and αsyn.

2.3. Size of liposomes and nanodiscs

The sizes of liposomes and nanodiscs were assessed in a Nano ZS (Malvern Instruments, Worcestershire, UK) at 35 °C, using a He—Ne laser at wavelength of 633 nm as source of incident light and scattering angle of 173°.

2.4. Protein preparation

The protein sequences can be found in Fig. 1. pT7-7 αsyn WT was a kind gift from Hilal Lashuel (Addgene plasmid # 36046; http://n2t.net/addgene:36046; RRID: Addgene_36,046). pT7-7 αsyn WT was transformed into the *E. coli* strain BL21(DE3) Star. A single transformed BL21 (DE3) colony harboring the recombinant pT7-7 vector was used to inoculate 100 mL LB broth containing 100 mg/L ampicillin in a flask and incubated overnight at 37 °C with shaking. 20 mL of culture were transferred to a 2 L flask containing 500 mL of fresh LB. The culture was grown with 160 rpm shaking at 37 °C until the OD (600 nm) reached 0.6. The culture was induced with 0.5 mM isopropyl-β-D-thiogalactopyranoside (IPTG). Cells were harvested by centrifugation (20 min at 4000*g*) at 4 h post-induction. The protein purification protocol followed previously published protocols with modifications [55]. Briefly, a pellet from a 1L culture was resuspended in 15 mL lysis buffer (10 mM Tris-HCl, 1 mM EDTA, pH 8.0, 1 mM phenylmethanesulfonyl fluoride (PMSF)) on ice, lysed by three freeze-thaw (N_2) cycles and sonicated 3 times using a Branson Sonifier 250 (Branson, Danbury, CT, USA), set at 50% duty cycle and 50% output (15s pulse; 1min rest). The cell lysate was boiled for 20 min and centrifuged at 4 °C, at 25200 *g* for 30 min. Streptomycin sulfate (10 mg/mL final concentration) was added to the supernatant, the solution was stirred for 15 min at 4 °C and centrifuged for 30 min at 25,200 *g*. Ammonium sulfate (0.36 mg/mL final concentration) was added to the supernatant, the solution was homogenized (by stirring for 15 min at 4 °C) and then centrifuged at 20600 *g* for 30 min at 4 °C [55]. The pellet was resuspended in 25 mM Tris-HCl, pH 7.4, filtered through a 0.22-μm membrane, and loaded onto a pre-equilibrated 5 mL HiTrap Q HP column (GE Healthcare, Uppsala, Sweden). The protein was eluted with a linear gradient of 0–400 mM NaCl over 8 column volumes, using an ÄKTA purifier 10 (GE Healthcare, Uppsala, Sweden). After analysis by SDS-PAGE, fractions containing the recombinant protein were pooled. Purified αsyn (5 mL) was subjected to overnight dialysis against 1 L 50 mM sodium phosphate 50 mM NaCl, pH 7.4 buffer. After dialysis, αsyn was divided into 1 mg/mL aliquots, lyophilized, and stored at −80 °C until further use. Analytical gel filtration was performed on a Superose 12 10/300 (GE Healthcare, Uppsala, Sweden) in 25 mM Tris-HCl, 150 mM NaCl, pH 7.4 to evaluate the oligomeric state of the protein. Protein purity was assessed by SDS-PAGE (12%).

Lyophilized samples of αsyn variants from whale and elephant were produced as described [36,53]. Prior to experiments, the samples were solubilized in 50 mM phosphate, 50 mM NaF, pH 7.4 and centrifuged at 15000 *g* for 10 min. The concentration was measured by UV/Vis spectroscopy using $\varepsilon_{280} = 5600\ M^{-1}\,cm^{-1}$ [55,56].

2.5. Circular dichroism (CD) spectroscopy

CD measurements were carried out in a Jasco 815 spectropolarimeter equipped with a PFD 425S Jasco Peltier temperature controller system (Japan Spectroscopy Co., Tokyo) using a cell with 1mm optical length.

2.5.1. Protein secondary structure in the presence of lipids

Scans were performed in a wavelength range of 198–260 nm, with a bandwidth of 1.0 nm, response time of 2 s and scanning speed of 50 nm min^{-1}, at two temperatures 45 and 25 °C to obtain information on the importance of the lipid phase (gel and liquid crystalline) on αsyn secondary structure [57]. Each spectrum was the average of at least nine accumulations. The spectrum of liposomes and nanodiscs in buffer at the studied concentrations were run as blanks to be subtracted from the liposome/αsyn and nanodiscs/αsyn spectra. The spectrum of αsyn

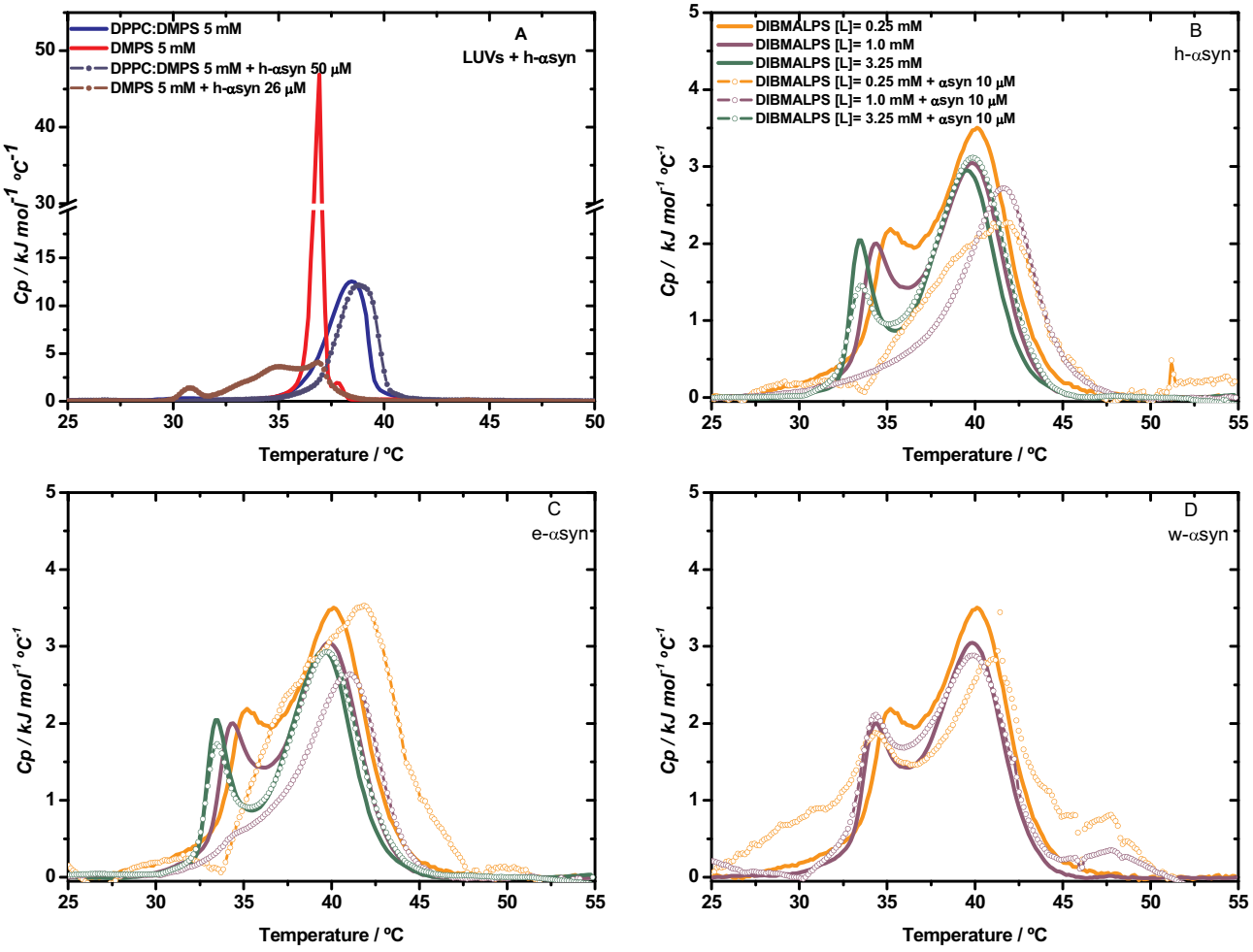

Fig. 3. Thermal profile of LUVs and DIBMALPS in the absence and in the presence of h-αsyn, e-αsyn, and w-αsyn variants. A: DPPC:DMPS 8:2 and DMPS LUVs with and without h-αsyn; B, C and D: DIBMALPs with and without 10 μM h-αsyn. DIBMALPs were prepared from 0.25, 1.0, and 3.25 mM of DPPC:DMPS (8:2) LUVs. For DIBMALPs (B, C, and D), the legend for the C and D curves is the same as in B.

in buffer at a protein concentration of 10 μM (concentration used in all protein/lipid experiments) was also recorded at the two studied temperatures. After blank correction, the observed ellipticity based on the total amount of protein in the mixture was converted to mean residue molar ellipticity (Θ, with units of degree cm^2 $dmol^{-1}$) using the Jasco 815 software. The αsyn/liposome and αsyn/nanodiscs mixtures were prepared immediately prior to each measurement. Lipid concentrations from 0.25 to 4.5 mM were used with liposomes and 0.25 to 3.25 mM with nanodiscs. Finally, CD measurements were also performed for mixtures of DIBMA copolymer and each of the three studied αsyn variants to assess the possibility of a direct polymer/protein interaction.

2.5.2. Thermally induced protein unfolding

To follow αsyn folding/unfolding process in the presence of lipids, the CD spectra were recorded at 208 and 222 nm, with a bandwidth of 2.0 nm, a response time of 4 s. performing successive up and down scans, in the temperature range of 20–55 °C, with increments of 1.0 °C min^{-1}. To ascertain the reversibility of the folding/unfolding process, spectra were recorded at 25 °C and 45 °C prior to temperature scan, and again at the end of the series of up and down scans.

2.6. Differential scanning calorimetry (DSC)

Differential scanning calorimetry (DSC) was performed on a VP-DSC (Malvern Instruments, UK). Experiments were performed with LUVs of DMPS and DPPC:DMPS 8:2 as well as with the DIBMALPs formed from DPPC:DMPS 8:2, for all the polymer/lipid mixtures prepared. The thermal behavior of mixtures of αsyn and LUVs or DIBMALPs was also followed by DSC. The sample mixtures were prepared immediately before the DSC run by adding the desired amount of αsyn stock solution to the liposomes or DIBMALPs. All procedures regarding sample preparation and handling (lag time at low temperature, the time between mixture, and the start of the experiment) were kept identical across all experiments to ensure that all samples had the same thermal history. The OriginLab software was used for baseline subtraction and for calculation of the gel-to-liquid crystalline phase transition temperature (T_m) and transition enthalpy (ΔH). In all cases, at least three successive up-scans were performed for each sample, at a scanning rate of 1.0 °C min^{-1} over a temperature range of 15–55 °C. The results reported are always for the second scan. The first scan frequently differs from subsequent ones, as the first passage across the thermotropic phase transition during the first scan allows for better "annealing" of the lipid bilayer. For the present system, we found that the calorimetric tracings were always similar from the second scan onwards.

After obtaining the enthalpy of the transition as the area of the transition peak (usually called the calorimetric enthalpy, ΔH_{cal}), the van't Hoff enthalpy (determined by the shape of the transition peak ($\Delta H_{vant'Hoff}$) was calculated as $\Delta H_{van'tHoff} = \frac{4 \times R \times T_m^2 \times C_{p,max}(T_m)}{\Delta H_{cal}}$, where R is the gas constant, T_m the transition temperature and $C_{p,\,max}(T_m)$ the value of C_p at T_m. The number of lipids per cooperative unit at the phase transition was obtained from the ratio of the enthalpies, $\Delta H_{vant'\,Hoff}/\Delta H_{cal}$.

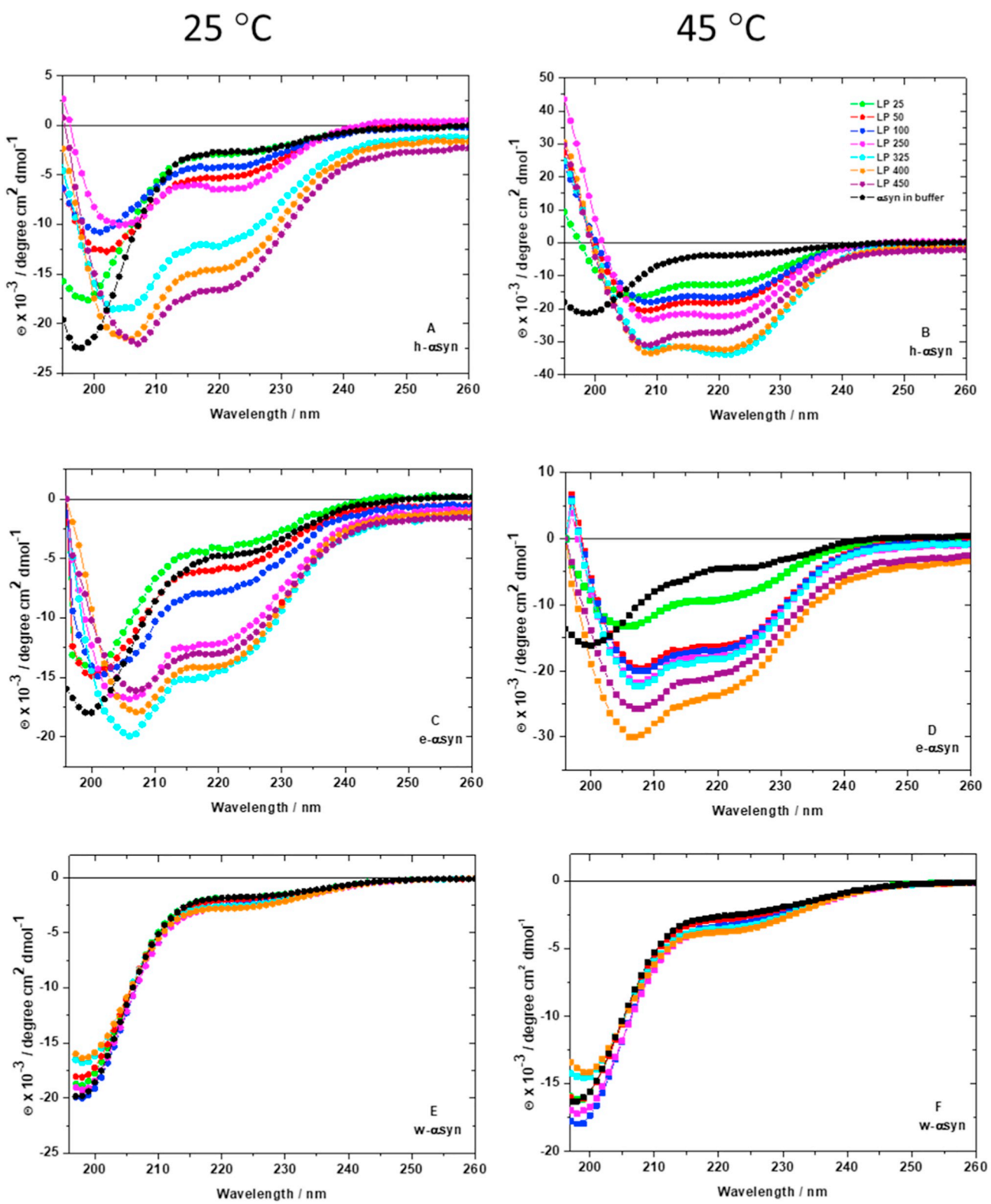

Fig. 4. Secondary structure of αsyn variants in the presence of LUVs of DMPS monitored by CD. The measurements were carried out using a constant protein concentration (10 μM) and increasing lipid to protein (LP) ratios at 25 °C (gel phase) and 45 °C (fluid phase). The identification of the curve for αsyn as well as for the lipid/protein ratios used can be found in panel B.

2.7. Nuclear magnetic resonance spectroscopy (NMR)

Increasing concentrations (0.5, 1.0, 2.5 and 3.25 mM) of DIBMA, DMPS; DPPC:DMPS 8:2 LUVs or DIBMALPs were added to samples containing 15 μM αsyn in phosphate buffer. D_2O 10% (*v*/v) was included in the sample buffer as a lock signal. NMR measurements were performed on a Bruker Avance III 400 spectrometer operating at a ^1H frequency of 400.1 MHz, at temperatures of (25 °C or 45 °C), depending on the experiment. ^1H saturation transfer difference (STD) NMR experiments [58] were acquired with a standard pulse sequence,

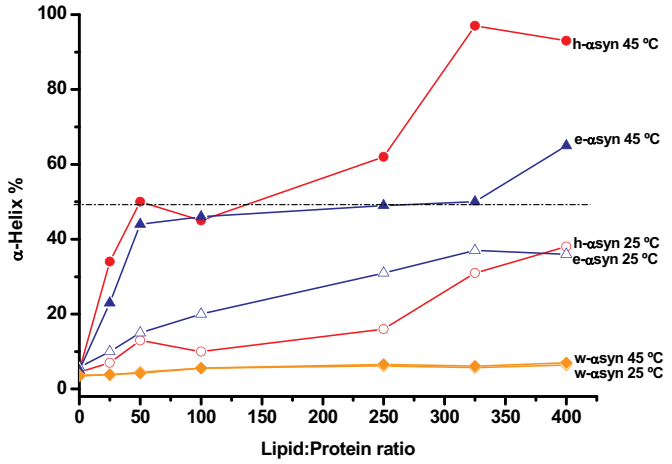

Fig. 5. The plot of the obtained values (Eqs. (1)–(3)) for the fraction of helical secondary structure (f_{helix}, in %) formed by each αsyn variant in the presence of DMPS LUVs as a function of LP ratio. The estimated uncertainty of each value is ± 10%.

employing shaped pulses for protein saturation and water suppression, z gradients for excitation sculpting, and spin-lock (T1ρ) filtering for background suppression. ^{1}H 1D NMR spectra were first collected for αsyn, DIBMA, DMPS and DPPC:DMPS liposomes and nanodiscs. The downfield amide region (> 7.0 ppm) showed protein resonances exclusively and, therefore, was chosen as the ideal region to selectively saturate protein signals but not DIBMA or lipid signals. Hence, ^{1}H-selective on-resonance irradiation of the protein signals was performed at 8.35 ppm using a 50-ms Eburp2,1000 shape pulses, and a saturation delay of 3 s. The STD experiments collected report the subtracted spectrum, in which the protein was selectively saturated (on-resonance spectrum) from one recorded without protein saturation (off-resonance spectrum). The difference spectrum shows only the signals of the binding entities that received saturation transfer from the protein, *via* spin diffusion, through the nuclear Overhauser effect (NOE), enabling the identification of direct binding.

Because of the observed similarities among the αsyn variants together with the stronger interaction and wider interest of the human variant, we performed NMR studies only with h-αsyn.

3. Results and discussion

We first describe the production and subsequent characterization of DIBMALPs made from polymer-mediated solubilization of LUVs composed of DPPC and DMPS, DPPC:DMPS (8:2). This lipid mixture was selected for three reasons: (i) 80% PC and 20% PS in the model membranes resembles the charge distribution in synaptic vesicles [59]. (ii) Its relatively high gel-to-fluid phase transition temperature (38.5 °C) allowed us to follow lipid phase transitions in nanodiscs by DSC. (iii) Although DMPS is known to efficiently induce α-helix formation in αsyn [11,17], pure DMPS lipid particles display an unphysiologically high charge density and, furthermore, lead to low liposome solubilization efficiencies by DIBMA due to electrostatic repulsion.

Unlike SMA [47], DIBMA shows very low absorption in the far-UV spectrum. This allowed us to use DIBMALPs to follow αsyn association and secondary-structure formation, in parallel with similar experiments performed with LUVs of DPPC:DMPS and DMPS. In this way, we could assess the differences in behavior depending on membrane charge (DMPS *vs* DPPC:DMPS 8:2) and lipid particle size (LUVs *vs* DIBMALPs).

3.1. Size of LUVS and DIBMALPs

The sizes in terms of *z*-average diameters obtained by DLS for the diameter (*d*) of our samples were ~140 nm for DMPS LUVs and ~110 nm for DPPC:DMPS (8:2) LUVs. Polydispersity indices were always in the range of 0.05–0.08. DIBMALPs at lipid concentrations of 0.25, 0.5, 1.0; 2.5, and 3.25 mM had a *z*-average diameter between 26 and 31 nm (see Table S1 Supporting information). Of note, it has been reported that αsyn is associated with synaptic vesicles (30–40 nm size) of the human brain and that the protein can regulate the size of these vesicles in neurons [60,61].

3.2. Thermotropic profile of LUVs and DIBMALPS

The DSC results for LUVs of DMPS, DPPC:DMPS 8:2, and DIBMALPs with 0.25, 1.0 and 3.25 mM lipid in the absence of αsyn are shown in Fig. 2. Associated thermodynamic parameters are provided in Table 1.

For DMPS, a sharp phase transition was observed, as expected for these single-lipid liposomes, centered at 36.9 °C (Table 1), a value close to the one observed by Galvagnion et al. [11], considering that we used LUVs (d~140 nm) and they used SUVs (diameter ~20 nm), and a lower concentration buffer, lower pH and no adjusted ionic strength. The mixed lipid system, DPPC:DMPS 8:2 showed a broader transition, but still with a single peak. By contrast, DIBMALPs ($C_{(DIBMA)}/C_{(DPPC:DMPS)}$ = 0.3) containing the DPPC:DMPS 8:2 mixture gave rise to two transitions, one below and one above the T_m of the corresponding lipid-only system. As regarding the effect of lipid concentration variation (keeping the same DIBMA/lipid ratio), we can see that the T_m are not affected (within the reported uncertainty), whereas there is a small decrease in both ΔH_1 and ΔH_2 only at the highest lipid concentrations.

It is possible that both the gel and fluid bilayer phases do not have the same properties in lipid-polymer nanodiscs as they have in LUVs. It is well known that, within a given lipid phase, there are a number of possible states of the lipids that belong to that phase, in terms of acyl chain order parameter, lateral diffusion, area per lipid group, *etc.* If one or both lipid phases are changed, then the transition gel(1) – to - L_α(1) can be different from the corresponding gel(2) -to-L_α (2). This can be the reason for the significantly different values of the enthalpy change (ΔH) observed for the gel-to-fluid phases for DPPC:DMPS 8:2 and the derived DIBMALPs (Table 1).

To obtain further information from DSC on differences between the studied systems, we estimated the number of lipids per cooperative unit at the phase transition for each system from the ratio of the enthalpies, $\Delta H_{vant' Hoff}/\Delta H_{cal}$. The values thus obtained were 233 in DMPS LUVs, 37 in DPPC:DMPS LUVs, and 19 in DIBMALPS (overall value). These results appear reasonable, given that we expected a higher number of lipids per cooperative unit for single-lipid LUVs made of negatively charged lipids only, a significantly smaller value for LUVs of DPPC:DMPS 8:2 consistent with a reduction in charge (*i.e.*, less repulsion from the lipid headgroups), and finally an even smaller value for DIBMALPs, which are smaller in overall size. Further, the value now obtained for DIBMALPs containing DPPC:DMPS 8:2 is of similar magnitude as the one reported previously by Oluwole et al. [46] for DMPC DIBMALPS (25 lipids per cooperative unit).

We rationalize the splitting into two peaks observed for DIBMALPS (Fig. 2) as follows. Our DLS results demonstrated a unimodal size distribution of DIBMALPs, and time-resolved Förster resonance energy transfer (TR-FRET) experiments have recently shown [41,43] fast lipid exchange among nanodiscs. Thus, while all nanodiscs are alike (at least, on the slow timescale of a DSC experiment), each nanodisc harbours different lipid populations. Based on the observed temperatures and the T_m of the pure lipid components, we hypothesize that one lipid population is close to the perimeter of the nanodisc that is more affected by the polymer rim (richer in DPPC, consistent with the higher T_m) and another one in the center of the nanodisc that is hardly affected by the polymer (rich in DMPS, again consistent with a lower T_m and the negative charge of DMPS, that we observed cannot alone form lipid nanodiscs with DIBMA). The observed decrease in ΔH in DIBMALPs can be the consequence of a more ordered (closer packed chains) fluid phase in

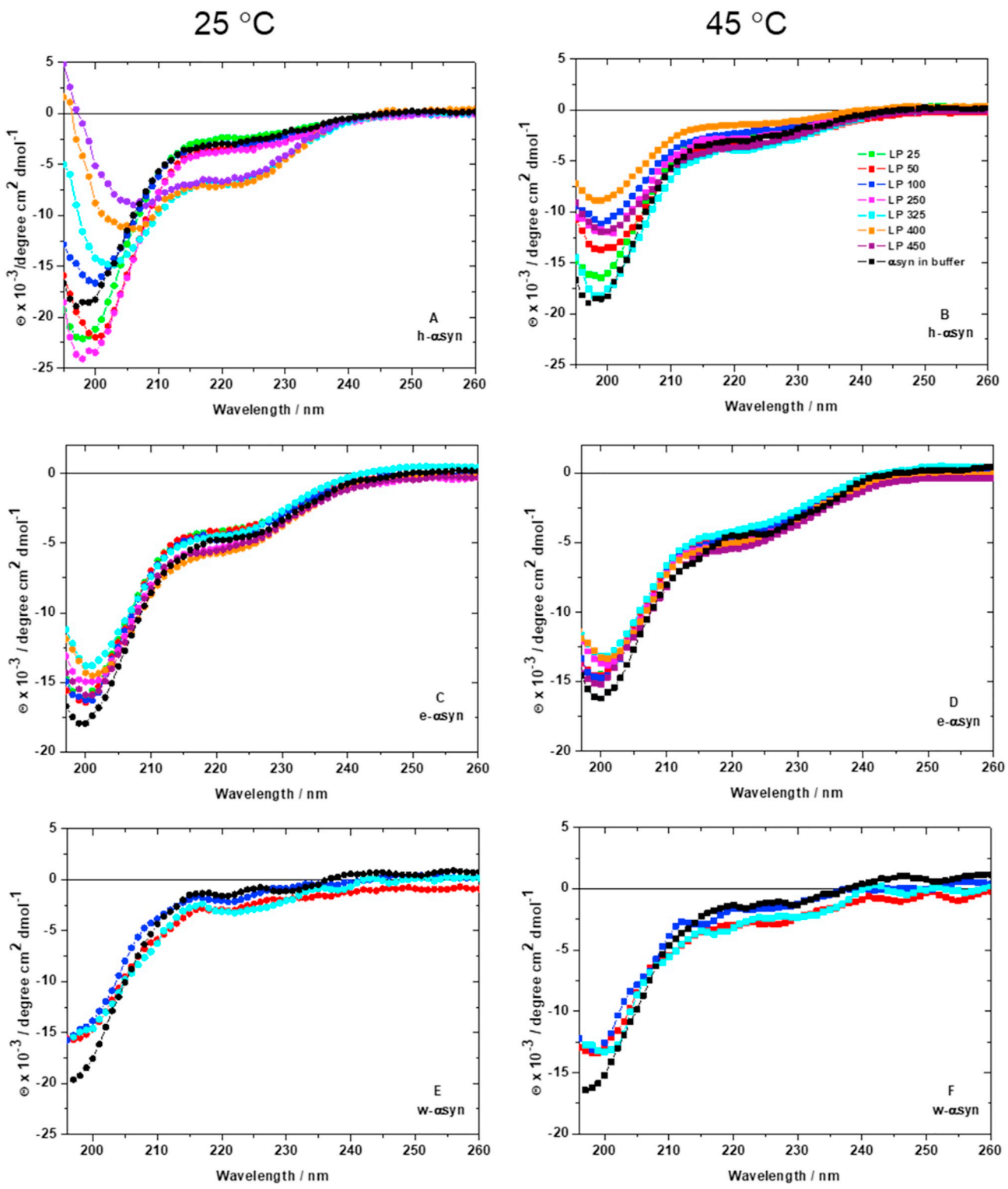

Fig. 6. Secondary structure of the three αsyn variants in the presence of LUVs of DPPC:DMPS 8:2 monitored by CD. The measurements were carried out using a constant protein concentration (10 μM) and increasing lipid/protein ratios (LP) at 25 °C (gel phase) and 45 °C (fluid phase). The identification of the curve for αsyn as well as for the used lipid/protein ratios is found in panel B.

the lipid nanodiscs as compared with the LUVs of DPPC:DMPS 8:2.

3.3. The presence of the protein changes the packaging of the nanodiscs

We performed DSC scans to observe the effect of αsyn on the thermotropic profile of LUVs (DMPS and DPPC: DMPS) and DIBMALPS. All three αsyn variants were tested with DIBMALPs, whereas only h-αsyn was run with LUVs. The presence of h-αsyn drastically changed the lipid transition profile of DMPS LUVs and, to a smaller extent, that of DIBMALPs, whereas DPPC:DMPS LUVs were rather insensitive to its presence (Fig. 3A–D).

In the presence of h-αsyn, the DMPS DSC profile changed significantly, with three peaks becoming apparent (Fig. 3A). This is compatible with a strong association of the protein with the negatively

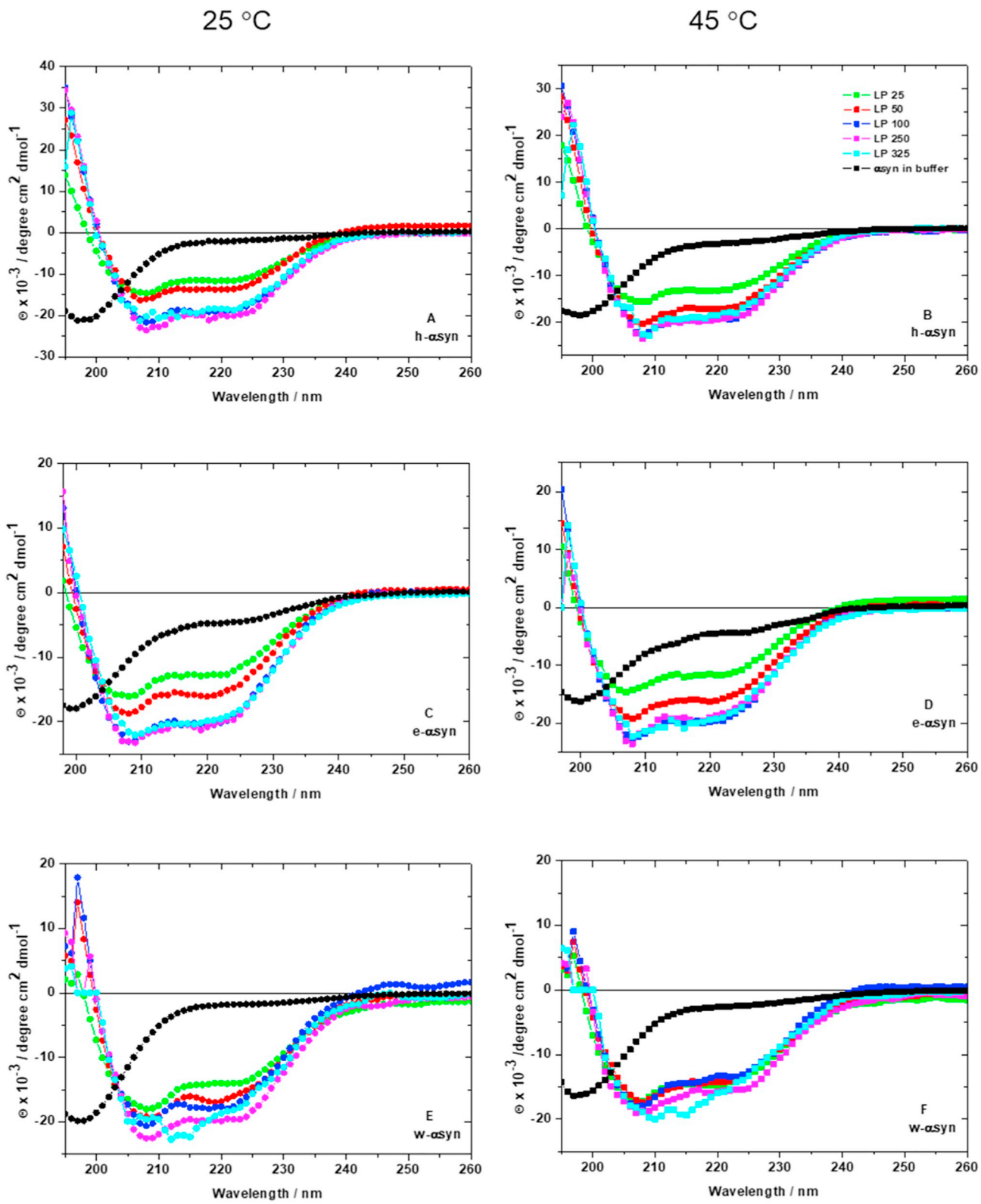

Fig. 7. Secondary structure of the three αsyn variants in the presence of DIBMALPS monitored by CD. Measurements were carried out using a constant protein concentration (10 μM) and increasing lipid to protein ratios (LP) at 25 °C (gel phase) and 45 °C (fluid phase). DIBMALPS were prepared from 0.25, 0.5, 1.0, 2.5, and 3.25 mM DPPC:DMPS (8:2) LUVs. A legend indicating the lipid/protein ratios used can be found in panel B.

charged lipid DMPS, and the peak splitting can be interpreted as reflecting the presence of different lipid/protein populations. The peak at higher temperature, ~37 °C, is probably mostly lipid-free protein population (T_m for pure DMPS is 36.9 °C), and the other two peaks, at lower temperatures (~35 and 31 °C) correspond to lipids closely associated with protein, with increasing protein contents. αsyn is known to preferentially associate with negatively charged phospholipids [10,32], and a strong effect and a similar peak splitting in DSC curves have been

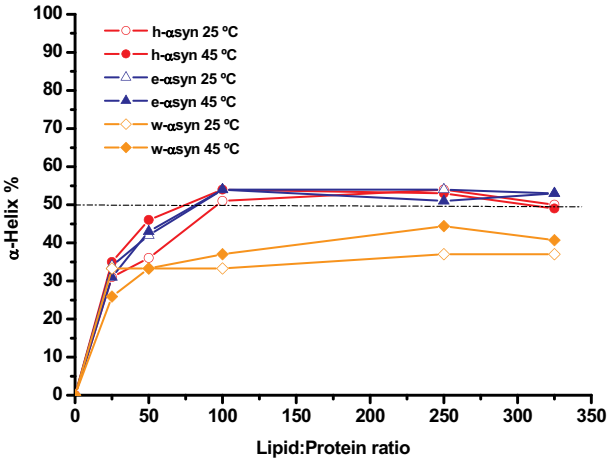

Fig. 8. The plot of the obtained values (Eqs. (1)–(3)) for the fraction of helical secondary structure (f_{helix}, in %) formed by each αsyn variant in the presence of DIBMALPs of DPPC:DMPS 8:2 as a function of LP ratio. The estimated uncertainty of each value is ± 10%.

Table 2
Dependence of the secondary structure of asyn on the parameters tested.

Parameters	h-αsyn	e-αsyn	w-αsyn
Lipid charge	+ + +	+ + +	*
Lipid temperature	+ + +	+ + +	*
Size of lipid system	–	–	+ +

+ + + to indicate higher sensitivity and – low sensitivity to the parameter.
* to indicate that the protein does not adopt a α-helical structure.

reported in a study involving h-αsyn and DMPS SUVs [11].

In the case of LUVs of DPPC:DMPS (Fig. 3A), the very modest effect observed is readily explained by the fact that the protein does not associate with zwitterionic lipids (results not shown). Furthermore, even a small reduction in the content of anionic lipid from 100% significantly reduces the binding affinity of h-αsyn [35], explaining why 20% DMPS was not enough to induce a significant change in the thermotropic phase transition. As regards DIBMALPs, we observed that for h-αsyn (Fig. 3B) and e-αsyn (Fig. 3C), the lower-temperature transition is not seen at low lipid/protein ratios (L:P 25 and L:P 100), whereas it was maintained at the highest lipid/protein ratio tested (L:P 325). Interestingly, none of these effects was apparent with w-αsyn, as the curves in the absence and presence of the protein were very similar (Fig. 3D). As we will see in the next section (CD results), this reflects the much weaker interaction of this synuclein variant with lipid membranes, as also reported earlier [53].

In view of all of these results, and considering the hypothesis raised above that exists a lipid population close to the perimeter of the nanodiscs that is rich in DPPC (with higher T_m) and another one in the center of the nanodiscs rich in DMPS (with lower T_m), the disappearance or change of the lower-temperature peak for h- and e-αsyn in the presence of the protein reflects α-helix formation and association of synuclein with the DMPS-rich part of the lipid nanodiscs. This could arise because interactions with the protein shift the equilibrium towards the fluid phase, raising its temperature, coinciding with the other peak, or it might become of two low enthalpy to be observed in DSC. Moreover, one could, at least in principle, also consider that helix formation is an exothermic process and phase transition an endothermic one, so they would tend to cancel out. This has been observed in peptide/lipid systems [62].

3.4. Lipid phase, charge, and size effects on the folding of αsyn

To assess the importance of charge fully negative liposomes (DMPS) *vs* partly negative (DPPC:DMPS 8:2), lipid phase (gel *vs* fluid), and size (LUVs *vs* DIBMALPs) on αsyn folding, we performed CD experiments with mixtures of one of the three αsyn (human, elephant, and whale) with LUVs of DMPS, DPPC:DMPS 8:2, and DIBMALPs at 25 and 45 °C (*i.e.*, below and above the phase transition temperature, respectively). The CD spectra of the three αsyn variants showed that they all assumed a predominantly random-coil structure in buffer under the conditions tested (Fig. 4). In the presence of DMPS LUVs at 45 °C, both h-αsyn and e-αsyn (Fig. 4B, D) formed an α-helix at all lipid concentrations (0.25 to 4.5 mM), whereas no secondary structure was induced in w-αsyn, irrespective of LP ratio (Fig. 4F). At 25 °C, the secondary structure induced by the negatively charged lipid surface was significantly decreased for both h-αsyn and e-αsyn (Fig. 4A, C). For LP 25 ([L] = 0.25 mM), 100 ([L] = 1.0 mM) and 250 ([L] = 2.5 mM) ratios, the proteins were still predominantly present as random coils (Fig. 4A, C). Only at LP 325 ([L] = 3.25 mM) and higher LP ratios, signatures of α-helix were detected, but the significantly lower values of molar ellipticity showed that the percentage of α-helix was much smaller when the lipid was in the gel phase.

In order to compare the α-helix contents of the three αsyn variants, we estimated the fraction of helix present (f_{helix}) at 25 and 45 °C by the observed ellipticity at 222 nm using Eqs. (1)–(3) below [63,64], where [Θ] is the molar ellipticity in degree cm^2 dmol^{-1} at 222 nm, n is the number of amino acid residues, k is a wavelength-dependent constant (k_{222} = 2.5), Θ_{helix}^{∞} is the maximum ellipticity of an α-helix with infinite length ($\Theta_{helix}^{\infty} = -40{,}000$ deg. cm^2 dmol^{-1}), and T is the temperature in °C.

$$f_{helix} = \frac{\Theta_{222} - \Theta_{coil}}{\Theta_{helix} - \Theta_{coil}} \quad (1)$$

$$\Theta_{helix} = \left[-\Theta_{helix}^{\infty}\left(1 - \frac{k}{n} + 100T\right)\right] \quad (2)$$

$$\Theta_{coil} = 640 - 45T \quad (3)$$

The estimates thus obtained from the experimental results are plotted in Fig. 5 as a function of LP ratio. Considering that we are using a single wavelength estimator to calculate the % of α-helix, the derived values have an estimated uncertainty of ± 10%. It is clear that the w-

Table 3
Values obtained for the partition coefficient, K_p (M^{-1}), and the lipid saturation mean residue molar ellipticity, $\Theta_{(lip,sat)}$, obtained by nonlinear regression of Eq. (4) to the mean residue molar ellipticity at 222 nm of mixtures of h-αsyn with DMPS LUVs or DIBMALPs.

Lipid systems	$\Theta_{(lip,sat)} \times 10^{-3}$ degree cm^2 dmol^{-1}	$K_p \times 10^{-3}$ (M^{-1})	$\Theta_{(lip,sat)} \times 10^{-3}$ degree cm^2 dmol^{-1}	$K_p \times 10^{-3}$ (M^{-1})
	25 °C		45 °C	
DMPS LUVs	–	–	−17 ± 1	7.0 ± 0.7[a]
DIBMALPS centrifuged	−32 ± 2	1.9 ± 0.6	−28 ± 2	3.2 ± 0.5
DIBMALPS not centrifuged	−28 ± 2	2.8 ± 0.6	−25 ± 2	4.1 ± 0.5

[a] The presented K_p values are based on the accessible lipid concentrations in each case – the lipid content in the outer leaflet for DMPS LUVs, and total lipid concentration for DIBMALPs.

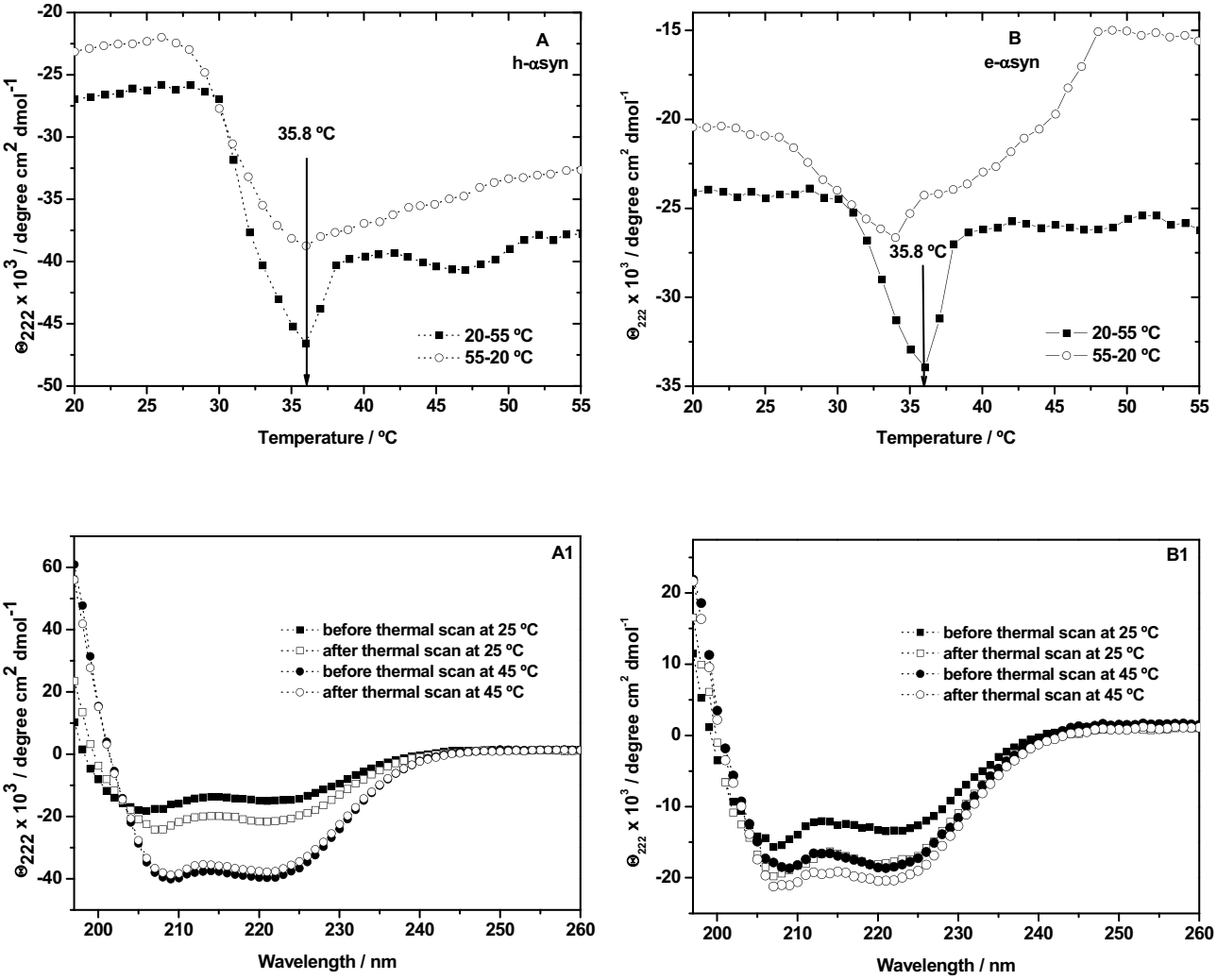

Fig. 9. Assessing the stability of αsyn folding. Forward (20–55 °C) and reverse (55–20 °C) thermal CD scans of human and elephant αsyn in presence of DMPS liposomes, performed at 222 nm. h-αsyn (*A*) and e-αsyn (*B*) both at 10 μM concentration in 4 mM DMPS liposome at lipid/protein = 400 (molar ratio). Before and after thermal scans a spectrum was recorded for the mixture at 25 and 45 °C to monitor the reversibility (A1 and B1).

αsyn variant has a very low percentage of secondary structure in the presence of DMPS LUVs, irrespective of L:P ratio and temperature, at odds with the other two variants. At 45 °C, h-αsyn and e-αsyn present similar values for the percentage of α-helix until LP 100, and thereafter h-αsyn has significantly higher helix content. At 25 °C, e-αsyn has a helix content somewhat higher than h-αsyn for some L:P ratios, but the differences are not considered significant, considering the low helix contents in the gel phase. Overall, the % of α-helix increases with L:P ratio until 350–400 for these two variants.

The induction of secondary structure in h-αsyn has also been tested by Kjaer et al. [35] by increasing the temperature in the presence of DMPG LUVs 200 nm. Similarly, to our observations with DMPS LUVs, the authors reported a maximum CD signal typical of α-helical structure in the lipid fluid phase; in addition, the dependence of αsyn affinity on DMPG vesicle size has been observed in that study.

A more recent study by Sahin et al. [53] in DMPG LUVs with the same αsyn variants has also demonstrated a weaker lipid binding affinity of whale and elephant αsyn compared with human αsyn, evidenced by lower α-helical content. Our results further show that w-αsyn is by far the least sensitive to vesicle charge and to lipid phase state but seems sensitive to the size and the curvature of the membrane-mimetic system used.

As described by the same authors [53] and others [24,65], despite their overall similarity in primary structure, the whale species has six mutations and a deletion (A53T, G68E, V95G, N103S, P108S, M116T, and Δ104) and the elephant species seven mutations (A53T, G68E, V95G, L100M, N103G, D115N, and M116V) when compared to human αsyn. Three of these mutations are common between whale and elephant αsyn, namely A53T, G68E, and V95G. The A53T mutation in humans is involved in Familial Parkinson's Disease, and the G68E is related to a lower propensity to form amyloid fibrils [65]. All three mutations are in the N-domain, which is the part involved in α-helical structural conformation, and thus this can modulate protein folding/aggregation in these species. Our results for the h-αsyn interaction with DMPS are also in agreement with the studies of Galvagnion et al. [11]. The authors performed CD experiments with DMPS SUVs (d = 20 nm) in the presence of αsyn and observed an increase in negative ellipticity at 222 nm when increasing the lipid concentration (0 to 12 mM) or the temperature (20 to 50 °C) until the values level off at what they call the saturation ellipticity. Similarly to our results on DMPS liposomes (d = 100 nm), they found the secondary structure of the protein to be favored in the fluid phase but did not observe any structure in the gel phase, in contrast with our results at the highest lipid concentrations (0.25 to 4.5 mM). Therefore, the size of lipid vesicles does not seem to affect αsyn-DMPS affinity, as also previously reported by Galvagnion *et al* [17]. Zhu & Fink [66] also found that the secondary structure was induced in both SUVs and LUVs vesicles of anionic phospholipids but point out that the α-helix content was higher in SUVs.

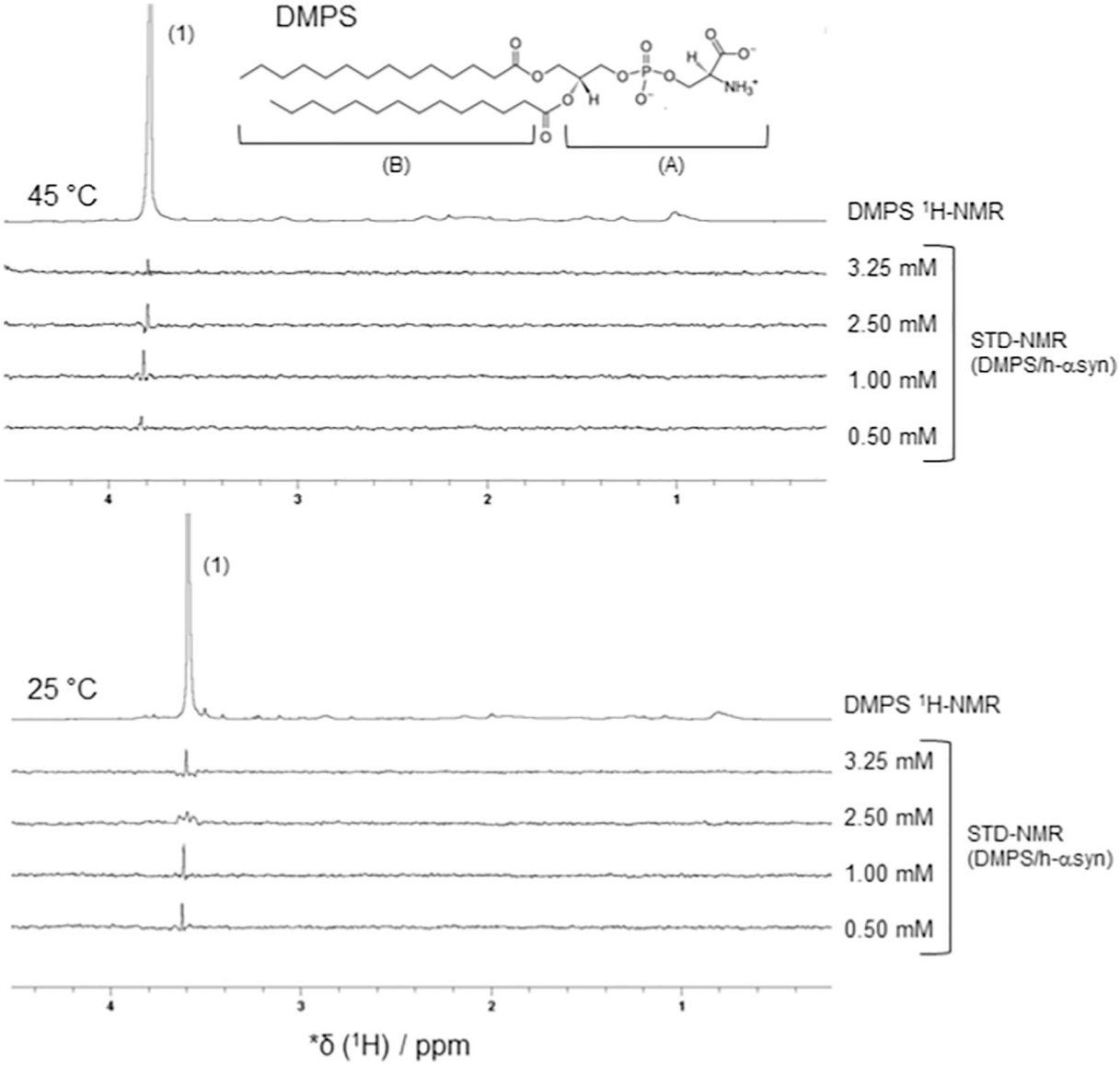

Fig. 10. ^{1}H 1D NMR and STD-NMR spectra of DMPS LUVs in the absence and presence of h-αsyn, at 25 and 45 °C, pH 7.4. The chemical structure of DMPS is shown, where region A relates to the polar head of the PS group (methylene protons – peak 1) and region B corresponds to the hydrophobic region of the molecule composed by the dimyristoyl hydrocarbon chains.

When LUVs of DPPC:DMPS 8:2 were used (only 20% negative charge), the behavior of the three αsyn variants was similar in the fluid phase at 45 °C (Fig. 6A–F), *i.e.*, the three proteins did not acquire any significant secondary structure, irrespective of the lipid concentration. In the gel phase at 25 °C, the same occurred for e-αsyn and w-αsyn, whereas for h-αsyn some change in conformation was detected, pointing to α-helix formation at the highest lipid/protein ratio (Fig. 6A), but with very low ellipticity values at 222 nm, indicating a weak association.

Several studies have found that, although αsyn does not adopt any secondary structure and only weakly associates with zwitterionic or neutral lipids, the presence of these lipids (LUVs and SUVs) reduces the rate of fibril formation and aggregation of h-αsyn [12,38,66,67], showing that the failure to induce secondary structure does not preclude other effects. Cell membranes comprise complex lipid mixtures, which might crucially affect the physiological functions and the pathophysiological effects of αsyn.

3.5. DIBMALPs modulate and stabilize αsyn secondary structure

The CD results for h-αsyn and its elephant and whale variants in the presence of DIBMALPs show remarkable features. In the presence of DIBMALPs, all three proteins adopted a well-defined α-helical structure, both in the gel and fluid phases of the lipid bilayer (Fig. 7).

Further, the existence of an isodichroic point is very clear for all αsyn variants, at ~203–204 nm, indicating a local two-state (α-helix, random coil) population in all variants, at odds with what was observed in the other lipids systems here studied, where the isodichroic point it was either not clear on non-existent, indicating that in those cases we might have a mixture of structures, whereas when DIBMALPs are used we only have αsyn random in solution or in helical form at the surface. Finally, the common point among the three variants is the similarity of the mean molar ellipticities in the presence of DIBMALPs nanodiscs.

We performed a similar calculation as above (Eqs. (1)–(3)), to estimate the α-helix content in each protein variant using the ellipticity observed at 222 nm, at both 25 and 45 °C when DIBMALPs were used. The results are presented as a plot of α-helix % as a function of lipid/protein ratio (Fig. 8).

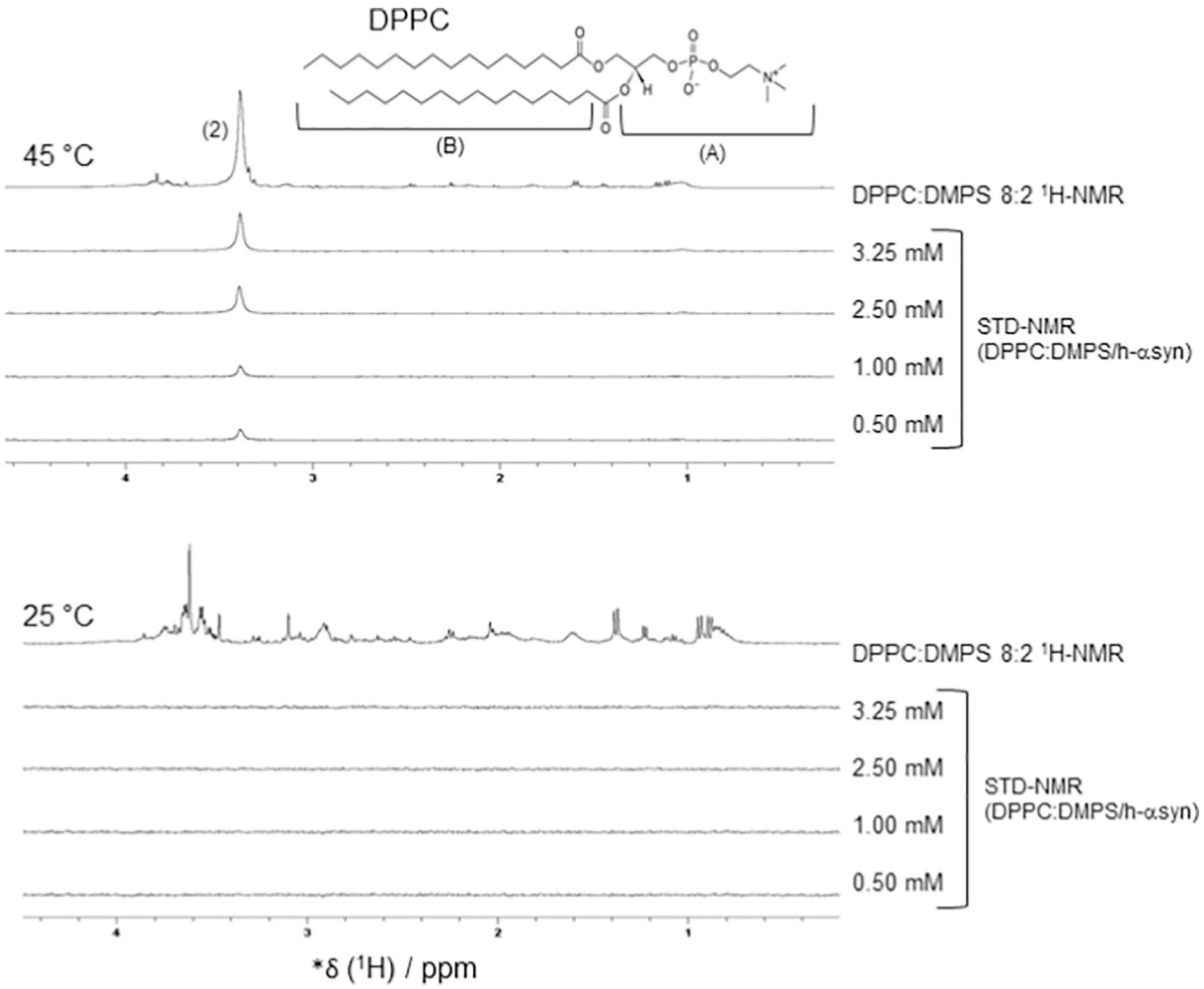

Fig. 11. ^{1}H 1D NMR and STD-NMR spectra of DPPC:DMPS 8:2 LUVs in the absence and presence of h-αsyn, at 25 and 45 °C, pH 7.4. The chemical structure of DPPC is shown, where region A relates to the polar head of the PC group (methyl choline groups ($-N^{+}(CH_3)_3$) – peak 2) and region B corresponds to the hydrophobic region of the molecule composed by the dipalmitoyl hydrocarbon chains.

h-αsyn and e-αsyn showed a more pronounced sensitivity to the lipid/protein ratio than w-αsyn but were rather insensitive to lipid phase. Accordingly, the α-helix content increased with increasing lipid concentration but did not change significantly with increasing temperature. As regards the elephant variant, the helix content was rather insensitive to either lipid concentration or temperature. Finally, although the whale protein exhibited the lowest helix contents, it did adopt an α-helical conformation in DIBMALPs, at odds with what we found in all other lipid systems and conditions tested.

In view of these results, we proceeded to test if the polymer alone could induce secondary structure, as it possesses negatively charged and hydrophobic moieties. We tested a relatively large span of polymer concentrations of 0.08–0.8 mM. In this concentration range, our CD results indicated that DIBMA induced helix formation of the human and elephant variants, but always to a smaller extent than in the presence of lipid-containing DIBMALPs. For whale αsyn, we did not observe any secondary-structure induction by the polymer alone. For h-αsyn, the helix formation was higher at 45 °C and increased with polymer concentration, but for e-αsyn it was insensitive to temperature and concentration. The calculated contents of α-helix were 25–40% for h-αsyn, and 20–30% for e-αsyn (data not shown). With that in view, although in the conditions we used we did not expect to have free polymer, we prepared DIBMALPs in the same way, but half of the preparation was centrifuged prior to addition of αsyn and perform the CD measurements (see Experimental section). Thereafter we compared the CD results obtained for h-αsyn/DIBMALPs of centrifuged and non-centrifuged samples. No difference was found between the two preparations, neither in the helix formation content nor in its thermal stability, as the tracings were superimposable under all conditions, that is, at different lipid concentrations and before and after the temperature ramp. Thus, the high efficiency of DIBMALPs is not due to a direct effect of free DIBMA but results from interactions of the proteins with lipid-bilayer nanodiscs.

One possible reason for their efficiency might be the small size of the DIBMALPs, together with their stability. While SUVs of similar size (~40 nm) can be prepared, it is well known that while they are stable above T_m, they tend to fuse into larger lipid aggregates at lower temperatures [65]. By contrast, DIBMALPs are stable, keeping their size for many days (at least one week, according to our DLS follow up results). Another possibility is that the diisobutylene groups penetrate between the hydrocarbon chains, whereas negatively charged maleic acid groups would point towards the solvent, leading to a strong and stable negatively charged belt surrounding the lipids. This would provide the nanodiscs with a highly negatively charged surface, explaining the secondary structure enhancement. Nevertheless, the w-αsyn results showed that charge was not the only important driving force, as the protein w-αsyn did not fold in the presence of DMPS, where it faced a fully negatively charged surface.

A third possibility is that the lys-rich 11-aa repeats found in the N-terminal are implicated in the formation of the α-helix, mediating the

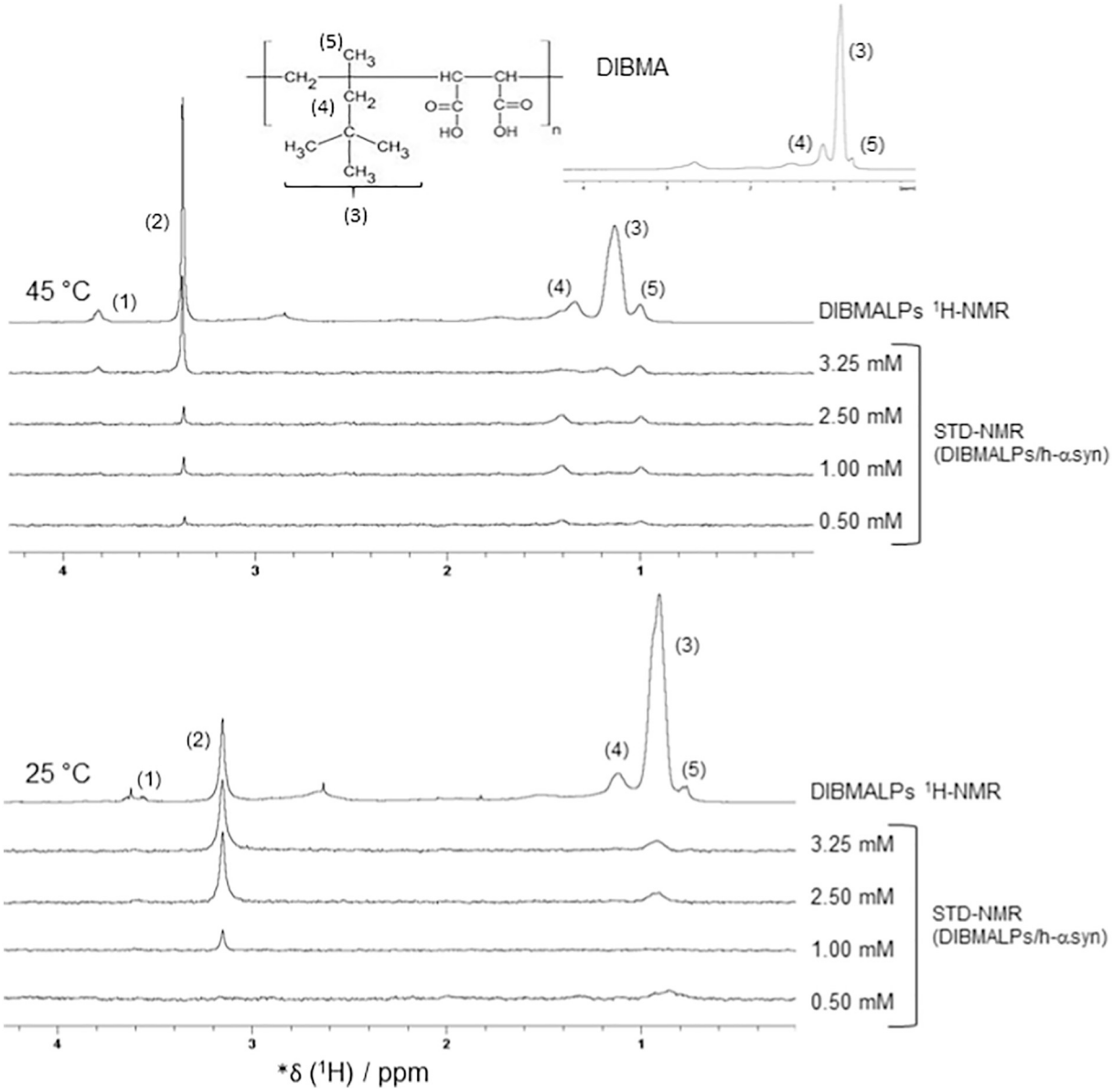

Fig. 12. 1D ^{1}H NMR and STD-NMR spectra of DIBMALPs nanodiscs in the absence and presence of h-αsyn, at 25 and 45 °C, in phosphate buffer, pH 7.4. 1D ^{1}H NMR spectrum of 3.5 mM DIBMA, pH 7.4 (inset). Molecular representation of DIBMA monomers is shown.

interactions with lipid membranes. The helix formed is amphipathic and has been considered similar to the one observed in apolipoproteins [6]. DIBMA has diisobutylene (hydrophobic) and maleic acid (hydrophilic) moieties [47], and lysine is a basic amino acid with a flexible hydrocarbon side chain [68]. The molecular structure of both compounds enables them to interact through both electrostatic and hydrophobic contacts. The interplay between interactions with lipids, DIBMA, and lysine side chains on the protein could form the ideal platform to fold and maintain the α-helix in αsyn. In Table 2 are summarized our findings in terms of parameters affecting the propensity to adopt an α-helical structure.

Our findings are in line with those previously reported for the interaction of h-αsyn with lipid nanodiscs assembled with membrane scaffold proteins (MSP) [33]. Their NMR spectra also showed that h-αsyn did not interact with zwitterionic lipid nanodiscs assembled with MSP, in either the gel phase or fluid phase, and that the interaction increased when the content of negative charge in the nanodiscs increased (from binary mixture of zwitterionic/negatively charged to 100% negatively charged lipids). In addition to the charge, the lipid fluidity of MSP nanodiscs was pivotal to modulate lipid-αsyn interaction. They further showed that the N-terminal is more sensitive to nanodiscs lipid charge, followed by the central region (non-amyloid component-NAC) and lastly by the C-terminal. At 100% negatively charged lipid, the protein is fully membrane bound.

In order to further quantify and compare the extent of synuclein partitioning into vesicles and DIBMALPs, we used the CD signal at 222 nm for mixtures of h-αsyn and DMPS LUVs or DIBMALPS (centrifuged and non-centrifuged) to calculate the partition coefficient, K_p (M^{-1}), and the value for the lipid saturation mean residue molar ellipticity, $\Theta_{(lip,sat)}$. Nonlinear regressions were performed according to Eq. (4):

$$\Theta_{(Lip)} - \Theta_{(free)} = \frac{(\Theta_{(lip,sat)} - \Theta_{(free)}) \times K_p\,[Lip]}{1 + K_p \times [Lip]} \quad (4)$$

where $\Theta_{(Lip)}$ is the mean residue molar ellipticity in the presence of a certain lipid concentration, $\Theta_{(lip,sat)}$ is the lipid saturation mean residue molar ellipticity and $\Theta_{(free)}$ is the mean residue molar ellipticity of the protein in the buffer. The binding curves for the DMPS LUVs were

calculated on the basis of the lipid concentration in the outer leaflet, while for the DIBMALPS nanodiscs we considered the total lipid content (the K_p value for DMPS based on total lipid content would be 3.5×10^3) (Table 3).

Although the partition constants were smaller for DIBMALPs at both temperatures, the lipid saturation mean residue molar ellipticity ($\Theta_{(lip,sat)}$) was always more negative, indicating that a higher degree of secondary structure exists in the presence of DIBMALPs. It should be noted that, the CD curves for centrifuged and non-centrifuged samples are superimposable (results not shown), and although the K_p values seem somewhat larger and the lipid saturation mean residue molar ellipticity, $\Theta_{(lip,sat)}$, smaller for the non-centrifuged samples, they agree within uncertainty. Therefore, a small effect of free polymer on the helix formation cannot be totally ruled out for h-αsyn, although if it exists, the effect is very small, as discussed above.

3.6. The α-helical structure of αsyn in the presence of LUVs and nanodiscs is thermally resistant

Moreover, in order to test the thermal stability of the secondary structure in DMPS LUVs and DIBMALPs, CD scans were performed in the same temperature range as our DSC runs (Fig. 9A, B), with h-αsyn and e-αsyn in LUVs of DMPS (L:P 400). The structure was found to be stable in both cases (Fig. 9A, B), and in fact the % of α-helix at 25 °C increased after thermal unfolding.

These experiments also allowed us to obtain the temperature for helix formation, evidenced by the decrease in the CD signal, that reaches a minimum value at 35.8 °C for both h-αsyn and e-αsyn. This temperature is not directly accessible by DSC because it has a very low enthalpy. Our results are in agreement with previous stability studies of h-αsyn and its elephant and whale variants in DMPG LUVs [53]. Interestingly, this value (35.8 °C) was found to be very close to the transition temperature of the lowest peak observed by DSC in DIBMALPs (see Table 1), T_{m1} ~35 °C, and thus reinforces our interpretation of the disappearance of this first peak in the presence of αsyn, as discussed in the DSC section.

3.7. Interactions characterized by saturation transfer difference (STD) NMR

Saturation transfer difference (STD) NMR is a fast and highly sensitive method of identifying direct binding *via* non-scalar magnetization transfer [58]. STD-NMR spectra at different DMPS, DPPC:DMPS 8:2 and nanodisc concentrations (0.5 to 3.25 mM), in the presence of a fixed concentration of h-αsyn, are shown in Figs. 10 to 12, respectively. Selective saturation of the protein signals in the amide region (8.35 ppm) enabled the identification of direct binding, both to DIBMA and phospholipids (DMPS and DPPC:DMPS 8:2), at both temperatures tested. When tested against DMPS LUVs solely, αsyn showed direct binding to the more flexible methylene groups associated with the polar head of DMPS (peak 1, region A) [69] at both 25 °C and 45 °C (Fig. 10). 1D ^{1}H NMR spectra of DMPS (Fig. 10 top spectrum at each temperature section and Fig. S1, Supplementary data) show upfield signals (0.0–2.0 ppm) assigned to methyl (-CH_3) and methylene (-CH_2) protons of the fatty acid chains (region B) and signals between 3.0 and 5.0 ppm that are attributed to glycerol protons and protons of the polar PS head (region A, Fig. S2, Supporting Information), as reported previously [69]. Additionally, in the gel phase (T = 25 °C < Tm), DMPS presents upfield signals of low intensity, due to the low mobility of the chains (small T_2, thus broader peaks, $\upsilon_{1/2} = 1/\pi T_2$, $\upsilon_{1/2}$ = width at half height); while in the liquid disordered phase (T = 45 °C > Tm), these upfield proton signals become sharper, due to the high mobility of the hydrocarbon chains (larger T_2, thus sharper peaks, $\upsilon_{1/2} = 1/\pi T_2$, $\upsilon_{1/2}$ = width at half height).

Likewise, direct binding was also identified *via* STD-NMR experiments when we monitored protein/lipid interactions between h-αsyn and DPPC:DMPS 8:2 LUVs (Fig. 11) and nanodiscs (Fig. 12). The presence of a higher proportion of DPPC in the liposomes stands out in the spectral region (1D ^{1}H NMR 3.25 mM DPPC:DMPS liposomes and nanodiscs reference spectra, Figs. 11 and 12, respectively) of the signals attributed to the lipids. A sharp and intense signal at 3.386 ppm (peak 2) assigned to the protons of the methyl choline groups (-$N^+(CH_3)_3$) of DPPC, as reported previously [70], is easily identified in both cases (Figs. 11 and 12). In what concerns Fig. 12 (DIBMALPs/αsyn), beyond peak 2 assigned to the methyl protons of the PC polar head (-$N^+(CH_3)_3$), less intense signals are also present at 3.624 ppm (25 °C) and 3.800 ppm (45 °C) (peak 1), that can be attributed to methylene protons of the phosphoserine (PS) group (region A).

Therefore, h-αsyn interacts with nanodiscs through direct binding to regions close to the polar heads of the phosphoserine (PS) and phosphocholine (PC) groups, at all concentrations tested, specially above the transition temperature (45 °C).

In addition, the upfield region (0. to 2.0 ppm, Fig. 12) shows intense signals attributed to the aliphatic groups of the polymer (peaks 3 to 5, Fig. 12). The inset in Fig. 12 shows the 1D ^{1}H NMR spectrum of 3.5 mM DIBMA in phosphate buffer. Peaks 3 to 5 in all spectra (Fig. 12) at both temperatures can therefore be attributed to DIBMA protons.

Hence, at 25 °C, the protein interacts with the nanodiscs mainly *via* involvement of the *tert*-butyl (peak 3, 0.904 ppm) (-$C(CH_3)_3$) group, whereas at 45 °C other regions of DIBMA seem to govern the interaction. At 45 °C, the signals attributed to the polymer (DIBMA) that report protein binding, are peaks 4 (1.335 ppm) and 5 (0.996 ppm) assigned to methylene (-CH_2) and methyl (-CH_3) groups, respectively. A rearrangement of the polymer region interacting with h-αsyn can be influenced by the phase transition of the lipid bilayer, explaining the differences observed between 25 °C and 45 °C.

Therefore, the STD-NMR experiments also show that beyond interacting with DMPS LUVs, h-αsyn is also able to interact with DPPC:DMPS 8:2 LUVs and much more efficiently with DIBMALPs, through a mechanism that favours protein folding *via* α-helix formation, as reported by the CD data. Given the resemblance with synaptic vesicles, the well-defined and mechanically stable DIBMALPs system described here can simulate relevant lipid-protein interactions that govern the process of structure acquisition and formation of nontoxic αsyn conformations *in vivo*.

4. Conclusions

Our studies revealed a new and promising application of polymer-encapsulated lipid-bilayer nanodiscs: aside from their use in membrane-protein extraction, we have demonstrated their excellent efficiency in structuring disordered proteins such as αsyn into nontoxic α-helical structures. This role of the polymer in stabilizing secondary structure needs to be further scrutinized. On a longer perspective, it is tempting to envisage a modified version of this polymer as a potential tool for inhibiting the aggregation of amyloidogenic proteins. Curiously, lysine residues have been targeted to study molecular tweezers, which are able to inhibit the aggregation of proteins in amyloidosis diseases [26–28].

Notes

The authors declare no conflicting interests.

Declaration of competing interest

The authors declare that they have no known competing financial interests or personal relationships that could have appeared to influence the work reported in this paper.

Acknowledgements

Thanks are due to Fundação para a Ciência e a Tecnologia (FCT), Portugal, for financial support to Projects UID/QUI/0081/2013 and PTDC/DTP-FTO/2784/2014, to FEDER (COMPETE 2020) for financial support to Norte-01-0145-FEDER-000028, including a Post-Doc grant to R. A., "Institute for Research and Innovation in Health Sciences" (POCI-01-0145-FEDER-007274) and Norte-01-0145-FEDER-000008 (NORTE 2020) Porto Neurosciences and Neurologic Disease Research Initiative at I3S. The NMR facility acknowledges the support of FEDER/COMPETE 2020 and FCT grants RECI/QEQ-QFI/0168/2012, CENTRO-07-CT62-FEDER-002012 and UID/QUI/00313/2019, and Rede Nacional de Ressonância Magnética Nuclear (RNRMN). This work was supported by the Deutsche Forschungsgemeinschaft (DFG) through grant KE 1478/4-1 to S.K. and the Carl Zeiss Foundation through the Centre for Lipidomics (CZSLip). D. E. O. gratefully acknowledges support from the Lundbeck Foundation (grants R180-2014-3545 and R276-2018-671) and the Danish Council for Independent Research, Medical Sciences (grant 4183-00225B). We thank Prof. Maria João Moreno for interesting discussions on the obtained results and Patrícia Martins for t*echnical assistance with the liposomes in the STD-NMR experiments* (Universidade de Coimbra), António Péon (CIQUP, Portugal) for producing the MD images for TOC and Bárbara Claro for help with its composition, and Annelize Z. B. Aragao (UNICAMP-Brazil) for technical assistance.

Appendix A. Supplementary data

Supplementary data to this article can be found online at https://doi.org/10.1016/j.bbamem.2020.183314.

References

[1] J.T. Bendor, T.P. Logan, R.H. Edwards, The function of α-synuclein, Neuron 79 (2013) 1044–1066, https://doi.org/10.1016/j.neuron.2013.09.004.
[2] L. Breydo, J.W. Wu, V.N. Uversky, α-Synuclein misfolding and Parkinson's disease, Biochim. Biophys. Acta Mol. basis Dis. 1822 (2012) 261–285, https://doi.org/10.1016/j.bbadis.2011.10.002.
[3] L. Maroteaux, J. Campanelli, R. Scheller, Synuclein: a neuron-specific protein localized to the nucleus and presynaptic nerve terminal, J. Neurosci. 8 (1988) 2804–2815, https://doi.org/10.1523/jneurosci.08-08-02804.1988.
[4] L. Maroteaux, R.H. Scheller, The rat brain synucleins; family of proteins transiently associated with neuronal membrane, Mol. Brain Res. 11 (1991) 335–343, https://doi.org/10.1016/0169-328X(91)90043-W.
[5] L. Stefanis, α-Synuclein in Parkinson's disease, Cold Spring Harbor Perspectives in Medicine, vol. 2, 2012, p. a009399, , https://doi.org/10.1101/cshperspect.a009399.
[6] R. Bussell, D. Eliezer, A structural and functional role for 11-mer repeats in α-synuclein and other exchangeable lipid binding proteins, J. Mol. Biol. 329 (2003) 763–778, https://doi.org/10.1016/S0022-2836(03)00520-5.
[7] K.K. Dev, K. Hofele, S. Barbieri, V.L. Buchman, H. van der Putten, Part II: α-synuclein and its molecular pathophysiological role in neurodegenerative disease, Neuropharmacology 45 (2003) 14–44, https://doi.org/10.1016/S0028-3908(03)00140-0.
[8] I. Dikiy, D. Eliezer, Folding and misfolding of alpha-synuclein on membranes, Biochim. Biophys. Acta Biomembr. 1818 (2012) 1013–1018, https://doi.org/10.1016/j.bbamem.2011.09.008.
[9] J. Burré, M. Sharma, T.C. Südhof, Cell biology and pathophysiology of α-synuclein, Cold Spring Harbor perspectives in medicine, 8 a024091. doi:https://doi.org/10.1101/cshperspect.a024091.
[10] W.S. Davidson, A. Jonas, D.F. Clayton, J.M. George, Stabilization of α-synuclein secondary structure upon binding to synthetic membranes, J. Biol. Chem. 273 (1998) 9443–9449, https://doi.org/10.1016/j.bbamem.2011.09.00810.1074/jbc.273.16.9443.
[11] C. Galvagnion, J.W.P. Brown, M.M. Ouberai, P. Flagmeier, M. Vendruscolo, A.K. Buell, E. Sparr, C.M. Dobson, Chemical properties of lipids strongly affect the kinetics of the membrane-induced aggregation of α-synuclein, Proc. Natl. Acad. Sci. U. S. A. 113 (2016) 7065–7070, https://doi.org/10.1016/j.bbamem.2011.09.00810.1073/pnas.1601899113.
[12] Z. Martinez, M. Zhu, S. Han, A.L. Fink, GM1 specifically interacts with α-synuclein and inhibits fibrillation, Biochemistry 46 (2007) 1868–1877, https://doi.org/10.1016/j.bbamem.2011.09.00810.1021/bi061749a.
[13] E.I. O'Leary, J.C. Lee, Interplay between α-synuclein amyloid formation and membrane structure, Biochim. Biophys. Acta, Proteins and Proteomics 1867 (2019) 483–491, https://doi.org/10.1016/j.bbapap.2018.09.012.
[14] A. Pineda, J. Burré, Modulating membrane binding of α-synuclein as a therapeutic strategy, Proc. Natl. Acad. Sci. U. S. A. 114 (2017) 1223–1225, https://doi.org/10.1073/pnas.1620159114.
[15] A. Rawat, R. Langen, J. Varkey, Membranes as modulators of amyloid protein misfolding and target of toxicity, Biochim. Biophys. Acta Biomembr. 1860 (2018) 1863–1875, https://doi.org/10.1016/j.bbamem.2018.04.011.
[16] M. Suzuki, K. Sango, K. Wada, Y. Nagai, Pathological role of lipid interaction with α-synuclein in Parkinson's disease, Neurochem. Int. 119 (2018) 97–106, https://doi.org/10.1016/j.neuint.2017.12.014.
[17] C. Galvagnion, A.K. Buell, G. Meisl, T.C.T. Michaels, M. Vendruscolo, T.P.J. Knowles, C.M. Dobson, Lipid vesicles trigger α-synuclein aggregation by stimulating primary nucleation, Nat. Chem. Biol. 11 (2015) 229–234, https://doi.org/10.1038/nchembio.1750.
[18] G. Young, N. Hundt, D. Cole, A. Fineberg, J. Andrecka, A. Tyler, A. Olerinyova, A. Ansari, E.G. Marklund, M.P. Collier, S.A. Chandler, O. Tkachenko, J. Allen, M. Crispin, N. Billington, Y. Takagi, J.R. Sellers, C. Eichmann, P. Selenko, L. Frey, R. Riek, M.R. Galpin, W.B. Struwe, J.L.P. Benesch, P. Kukura, Quantitative mass imaging of single biological macromolecules, Science 360 (2018) 423, https://doi.org/10.1126/science.aar5839.
[19] M. Bucciantini, G. Calloni, F. Chiti, L. Formigli, D. Nosi, C.M. Dobson, M. Stefani, Prefibrillar amyloid protein aggregates share common features of cytotoxicity, J. Biol. Chem. 279 (2004) 31374–31382, https://doi.org/10.1074/jbc.M400348200.
[20] J.I. Gallea, M.S. Celej, Structural insights into amyloid oligomers of the Parkinson disease-related protein α-synuclein, J. Biol. Chem. 289 (2014) 26733–26742, https://doi.org/10.1074/jbc.M114.566695.
[21] R. Porcari, C. Proukakis, C.A. Waudby, B. Bolognesi, P.P. Mangione, J.F.S. Paton, S. Mullin, L.D. Cabrita, A. Penco, A. Relini, G. Verona, M. Vendruscolo, M. Stoppini, G.G. Tartaglia, C. Camilloni, J. Christodoulou, A.H.V. Schapira, V. Bellotti, The H50Q mutation induces a 10-fold decrease in the solubility of α-synuclein, J. Biol. Chem. 290 (2015) 2395–2404, https://doi.org/10.1074/jbc.M114.610527.
[22] M. Terada, G. Suzuki, T. Nonaka, F. Kametani, A. Tamaoka, M. Hasegawa, The effect of truncation on prion-like properties of α-synuclein, J. Biol. Chem. 293 (2018) 13910–13920, https://doi.org/10.1074/jbc.RA118.001862.
[23] M. Andreasen, N. Lorenzen, D. Otzen, Interactions between misfolded protein oligomers and membranes: a central topic in neurodegenerative diseases? Biophys. Acta, Biomembr. 1848 (2015) 1897–1907, https://doi.org/10.1016/j.bbamem.2015.01.018.
[24] L.T. Hai-Ning Du, Xiao-Ying Luo, Hong-Tao Li, Jun Hu, Jia-Wei Zhou, Hong-Yu Hu, A peptide motif consisting of glycine, alanine, and valine is required for the fibrillization and cytotoxicity of human α-synuclein, Biochemistry 42 (2003) 8870–8878, https://doi.org/10.1021/bi034028+.
[25] C.L. Ugalde, V.A. Lawson, D.I. Finkelstein, A.F. Hill, The role of lipids in α-synuclein misfolding and neurotoxicity, J. Biol. Chem. (2019), https://doi.org/10.1074/jbc.rev119.007500.
[26] M. Perni, C. Galvagnion, A. Maltsev, G. Meisl, M.B.D. Müller, P.K. Challa, J.B. Kirkegaard, P. Flagmeier, S.I.A. Cohen, R. Cascella, S.W. Chen, R. Limbocker, P. Sormanni, G.T. Heller, F.A. Aprile, N. Cremades, C. Cecchi, F. Chiti, E.A.A. Nollen, T.P.J. Knowles, M. Vendruscolo, A. Bax, M. Zasloff, C.M. Dobson, A natural product inhibits the initiation of α-synuclein aggregation and suppresses its toxicity, Proc. Natl. Acad. Sci. U. S. A. 114 (2017) E1009–E1017, https://doi.org/10.1073/pnas.1610586114.
[27] J. Pujols, S. Peña-Díaz, D.F. Lázaro, F. Peccati, F. Pinheiro, D. González, A. Carija, S. Navarro, M. Conde-Giménez, J. García, S. Guardiola, E. Giralt, X. Salvatella, J. Sancho, M. Sodupe, T.F. Outeiro, E. Dalfó, S. Ventura, Small molecule inhibits α-synuclein aggregation, disrupts amyloid fibrils, and prevents degeneration of dopaminergic neurons, Proc. Natl. Acad. Sci. U. S. A. 115 (2018) 10481–10486, https://doi.org/10.1073/pnas.1804198115.
[28] S. Sinha, D.H.J. Lopes, Z. Du, E.S. Pang, A. Shanmugam, A. Lomakin, P. Talbiersky, A. Tennstaedt, K. McDaniel, R. Bakshi, P.-Y. Kuo, M. Ehrmann, G.B. Benedek, J.A. Loo, F.-G. Klärner, T. Schrader, C. Wang, G. Bitan, Lysine-specific molecular tweezers are broad-spectrum inhibitors of assembly and toxicity of amyloid proteins, J. Am. Chem. Soc. 133 (2011) 16958–16969, https://doi.org/10.1021/ja206279b.
[29] J. Burré, M. Sharma, T.C. Südhof, Definition of a molecular pathway mediating α-synuclein neurotoxicity, J. Neurosci. 35 (2015) 5221–5232, https://doi.org/10.1523/JNEUROSCI.4650-14.2015.
[30] C. Eichmann, S. Campioni, J. Kowal, I. Maslennikov, J. Gerez, X. Liu, J. Verasdonck, N. Nespovitaya, S. Choe, B.H. Meier, P. Picotti, J. Rizo, H. Stahlberg, R. Riek, Preparation and characterization of stable α-synuclein lipoprotein particles, J. Biol. Chem. 291 (2016) 8516–8527, https://doi.org/10.1074/jbc.M115.707968.
[31] M. Falke, J. Victor, M.M. Wördehoff, A. Peduzzo, T. Zhang, G.F. Schröder, A.K. Buell, W. Hoyer, M. Etzkorn, α-Synuclein-derived lipoparticles in the study of α-synuclein amyloid fibril formation, Chem. Phys. Lip. 220 (2019) 57–65, https://doi.org/10.1016/j.chemphyslip.2019.02.009.
[32] E. Jo, J. McLaurin, C.M. Yip, P. St, P.E. Fraser George-Hyslop, α-Synuclein membrane interactions and lipid specificity, J. Biol. Chem. 275 (2000) 34328–34334, https://doi.org/10.1074/jbc.M004345200.
[33] T. Viennet, M.M. Wördehoff, B. Uluca, C. Poojari, H. Shaykhalishahi, D. Willbold, B. Strodel, H. Heise, A.K. Buell, W. Hoyer, M. Etzkorn, Structural insights from lipid-bilayer nanodiscs link α-synuclein membrane-binding modes to amyloid fibril formation, Commun. Biol. 1 (2018) 44, https://doi.org/10.1038/s42003-018-0049-z.
[34] Z. Zhang, C. Dai, J. Bai, G. Xu, M. Liu, C. Li, Ca2+ modulating α-synuclein membrane transient interactions revealed by solution NMR spectroscopy, Biophys. Acta, Biomembr. 1838 (2014) 853–858, https://doi.org/10.1016/j.bbamem.2013.11.016.

[35] L. Kjaer, L. Giehm, T. Heimburg, D. Otzen, The influence of vesicle size and composition on alpha-synuclein structure and stability, Biophys. J. 96 (2009) 2857–2870, https://doi.org/10.1016/j.bpj.2008.12.3940.
[36] N. Lorenzen, S.B. Nielsen, A.K. Buell, J.D. Kaspersen, P. Arosio, B.S. Vad, W. Paslawski, G. Christiansen, Z. Valnickova-Hansen, M. Andreasen, J.J. Enghild, J.S. Pedersen, C.M. Dobson, T.P.J. Knowles, D.E. Otzen, The role of stable α-synuclein oligomers in the molecular events underlying amyloid formation, J. Am. Chem. Soc. 136 (2014) 3859–3868, https://doi.org/10.1021/ja411577t.
[37] B.S. Eichmann Cédric, Riek Roland, α-Synuclein lipoprotein nanoparticles, Nanotechnol. Rev. 6 (2017) 105–110, https://doi.org/10.1515/ntrev-2016-0062.
[38] Z. Jiang, M. de Messieres, J.C. Lee, Membrane remodeling by α-synuclein and effects on amyloid formation, J. Am. Chem. Soc. 135 (2013) 15970–15973, https://doi.org/10.1021/ja405993r.
[39] N. Mizuno, J. Varkey, N.C. Kegulian, B.G. Hegde, N. Cheng, R. Langen, A.C. Steven, Remodeling of lipid vesicles into cylindrical micelles by α-Synuclein in an extended α-helical conformation, J. Biol. Chem. 287 (2012) 29301–29311, https://doi.org/10.1074/jbc.M112.365817.
[40] J. Varkey, N. Mizuno, B.G. Hegde, N. Cheng, A.C. Steven, R. Langen, α-Synuclein oligomers with broken helical conformation form lipoprotein nanoparticles, J. Biol. Chem. 288 (2013) 17620–17630, https://doi.org/10.1074/jbc.M113.476697.
[41] R. Cuevas Arenas, B. Danielczak, A. Martel, L. Porcar, C. Breyton, C. Ebel, S. Keller, Fast collisional lipid transfer among polymer-bounded nanodiscs, Sci. Rep. 7 (2017) 45875, https://doi.org/10.1038/srep45875 https://www.nature.com/articles/srep45875#supplementary-information.
[42] R. Cuevas Arenas, J. Klingler, C. Vargas, S. Keller, Influence of lipid bilayer properties on nanodisc formation mediated by styrene/maleic acid copolymers, Nanoscale 8 (2016) 15016–15026, https://doi.org/10.1039/C6NR02089E.
[43] B. Danielczak, S. Keller, Collisional lipid exchange among DIBMA-encapsulated nanodiscs (DIBMALPs), Eur. Polym. J. 109 (2018) 206–213, https://doi.org/10.1016/j.eurpolymj.2018.09.043.
[44] B. Danielczak, A. Meister, S. Keller, Influence of Mg2+ and Ca2+ on nanodisc formation by diisobutylene/maleic acid (DIBMA) copolymer, Chem. Phys. Lipids 221 (2019) 30–38, https://doi.org/10.1016/j.chemphyslip.2019.03.004.
[45] A. Grethen, A.O. Oluwole, B. Danielczak, C. Vargas, S. Keller, Thermodynamics of nanodisc formation mediated by styrene/maleic acid (2:1) copolymer, Sci. Rep. 7 (2017) 11517, , https://doi.org/10.1038/s41598-017-11616-z.
[46] A.O. Oluwole, B. Danielczak, A. Meister, J.O. Babalola, C. Vargas, S. Keller, Solubilization of membrane proteins into functional lipid-bilayer nanodiscs using a diisobutylene/maleic acid copolymer, Angew. Chem., Int. Ed. Engl. 56 (2017) 1919–1924, https://doi.org/10.1002/anie.201610778.
[47] A.O. Oluwole, J. Klingler, B. Danielczak, J.O. Babalola, C. Vargas, G. Pabst, S. Keller, Formation of lipid-bilayer nanodiscs by diisobutylene/maleic acid (DIBMA) copolymer, Langmuir 33 (2017) 14378–14388, https://doi.org/10.1021/acs.langmuir.7b03742.
[48] M. Keane, J. Semeiks, A.E. Webb, Y.I. Li, V. Quesada, T. Craig, L.B. Madsen, S. van Dam, D. Brawand, P.I. Marques, P. Michalak, L. Kang, J. Bhak, H.-S. Yim, N.V. Grishin, N.H. Nielsen, M.P. Heide-Jørgensen, E.M. Oziolor, C.W. Matson, G.M. Church, G.W. Stuart, J.C. Patton, J.C. George, R. Suydam, K. Larsen, C. López-Otín, M.J. O'Connell, J.W. Bickham, B. Thomsen, J.P. de Magalhães, Insights into the evolution of longevity from the bowhead whale genome, Cell Rep. 10 (2015) 112–122, https://doi.org/10.1016/j.celrep.2014.12.008.
[49] R.M. Laws, Age criteria for the African elephant, African J. Ecol. 4 (1966) 1–37, https://doi.org/10.1111/j.1365-2028.1966.tb00878.x.
[50] S. Ma, V.N. Gladyshev, Molecular signatures of longevity: insights from cross-species comparative studies, Semin. Cell Dev. Biol. 70 (2017) 190–203, https://doi.org/10.1016/j.semcdb.2017.08.007.
[51] J.M. George, H. Jin, W.S. Woods, D.F. Clayton, Characterization of a novel protein regulated during the critical period for song learning in the zebra finch, Neuron 15 (1995) 361–372, https://doi.org/10.1016/0896-6273(95)90040-3.
[52] R. Jakes, M.G. Spillantini, M. Goedert, Identification of two distinct synucleins from human brain, FEBS Lett. 345 (1994) 27–32, https://doi.org/10.1016/0014-5793(94)00395-5.
[53] C. Sahin, L. Kjær, M.S. Christensen, J.N. Pedersen, G. Christiansen, A.-M.W. Pérez, I.M. Møller, J.J. Enghild, J.S. Pedersen, K. Larsen, D.E. Otzen, α-Synucleins from animal species show low fibrillation propensities and weak oligomer membrane disruption, Biochemistry 57 (2018) 5145–5158, https://doi.org/10.1021/acs.biochem.8b00627.
[54] F. Sievers, D.G. Higgins, Clustal omega for making accurate alignments of many protein sequences, Protein Sci. 27 (2018) 135–145, https://doi.org/10.1002/pro.3290.
[55] W. Hoyer, T. Antony, D. Cherny, G. Heim, T.M. Jovin, V. Subramaniam, Dependence of α-synuclein aggregate morphology on solution conditions, J. Mol. Biol. 322 (2002) 383–393, https://doi.org/10.1016/S0022-2836(02)00775-1.
[56] P.H. Weinreb, W. Zhen, A.W. Poon, K.A. Conway, P.T. Lansbury, NACP, a protein implicated in Alzheimer's disease and learning, is natively unfolded, Biochemistry 35 (1996) 13709–13715, https://doi.org/10.1021/bi961799n.
[57] N.J. Greenfield, Using circular dichroism spectra to estimate protein secondary structure, Nat. Protoc. 1 (2007) 2876, https://doi.org/10.1038/nprot.2006.202 (https://www.nature.com/articles/nprot.2006.202#supplementary-information).
[58] M. Mayer, B. Meyer, Characterization of ligand binding by saturation transfer difference NMR spectroscopy, Angew. Chem., Int. Ed. Engl. 38 (1999) 1784–1788, https://doi.org/10.1002/(sici)1521-3773(19990614)38:12<1784::Aid-anie1784>3.0.Co;2-q.
[59] J.H. Walker, D.V. Agoston, The synaptic vesicle and the cytoskeleton, Biochem. J. 247 (1987) 249–258, https://doi.org/10.1042/bj2470249.
[60] K.m. Harris, P. Sultan, Variation in the number, location and size of synaptic vesicles provides an anatomical basis for the nonuniform probability of release at hippocampal CA1 synapses, Neuropharmacology 34 (1995) 1387–1395, https://doi.org/10.1016/0028-3908(95)00142-S.
[61] D.D. Murphy, S.M. Rueter, J.Q. Trojanowski, V.M.-Y. Lee, Synucleins are developmentally expressed, and α-synuclein regulates the size of the presynaptic vesicular pool in primary hippocampal neurons, J. Neurosci. 20 (2000) 3214–3220, https://doi.org/10.1523/jneurosci.20-09-03214.2000.
[62] T. Silva, B. Claro, B.F.B. Silva, N. Vale, P. Gomes, M.S. Gomes, S.S. Funari, J. Teixeira, D. Uhríková, M. Bastos, Unravelling a mechanism of action for a cecropin A-melittin hybrid antimicrobial peptide: the induced formation of multilamellar lipid stacks, Langmuir 34 (2018) 2158–2170, https://doi.org/10.1021/acs.langmuir.7b03639.
[63] J.M. Scholtz, H. Qian, E.J. York, J.M. Stewart, R.L. Baldwin, Parameters of helix–coil transition theory for alanine-based peptides of varying chain lengths in water, Biopolymers 31 (1991) 1463–1470, https://doi.org/10.1002/bip.360311304.
[64] T. Wieprecht, M. Beyermann, J. Seelig, Thermodynamics of the coil–α-helix transition of amphipathic peptides in a membrane environment: the role of vesicle curvature, Biophys. Chem. 96 (2002) 191–201, https://doi.org/10.1016/S0301-4622(02)00025-X.
[65] M.H. Polymeropoulos, C. Lavedan, E. Leroy, S.E. Ide, A. Dehejia, A. Dutra, B. Pike, H. Root, J. Rubenstein, R. Boyer, E.S. Stenroos, S. Chandrasekharappa, A. Athanassiadou, T. Papapetropoulos, W.G. Johnson, A.M. Lazzarini, R.C. Duvoisin, G. Di Iorio, L.I. Golbe, R.L. Nussbaum, Mutation in the α-synuclein gene identified in families with Parkinson's disease, Science 276 (1997) 2045–2047, https://doi.org/10.1126/science.276.5321.2045.
[66] M. Zhu, A.L. Fink, Lipid binding inhibits α-synuclein fibril formation, J. Biol. Chem. 278 (2003) 16873–16877, https://doi.org/10.1074/jbc.M210136200.
[67] M. Zhu, J. Li, A.L. Fink, The association of α-synuclein with membranes affects bilayer structure, stability, and fibril formation, J. Biol. Chem. 278 (2003) 40186–40197, https://doi.org/10.1074/jbc.M305326200.
[68] S. Sokalingam, G. Raghunathan, N. Soundrarajan, S.-G. Lee, A study on the effect of surface lysine to arginine mutagenesis on protein stability and structure using green fluorescent protein, PLoS One 7 (2012) e40410, , https://doi.org/10.1371/journal.pone.0040410.
[69] A. Sanson, M.A. Monck, J.-M. Neumann, 2D 1H-NMR conformational study of phosphatidylserine diluted in perdeuterated dodecylphosphocholine micelles. Evidence for a pH-induced conformational transition, Biochemistry 34 (1995) 5938–5944, https://doi.org/10.1021/bi00017a023.
[70] R. Sinha, A. Joshi, U.J. Joshi, S. Srivastava, G. Govil, Localization and interaction of hydroxyflavones with lipid bilayer model membranes: a study using DSC and multinuclear NMR, Eur. J. Med. Chem. 80 (2014) 285–294, https://doi.org/10.1016/j.ejmech.2014.04.054.